Die approbierte gedruckte Originalversion dieser Diplomarbeit ist an der TU Wien Bibliothek verfügbar
The approved original version of this thesis is available in print at TU Wien Bibliothek.

TECHNISCHE UNIVERSITÄT WIEN

DIPLOMA THESIS

Using LA-ICP-MS for the Determination of Deuterium in an Effort to Analyze Water Absorption by Thin Polymer Films

submitted in satisfaction of the requirements for the degree of
Diplom-Ingenieur / Diplom-Ingenieurin
of the Technische Universität Wien (Vienna University of Technology), Faculty of Technical Chemistry

by

David Ken Gibbs
Matr.Nr.: 01616021

under the supervision of

Univ.-Prof. Dipl.-Ing. Dr.techn. **Andreas Limbeck**

Institute of Chemical Technologies and Analytics
Research Group for Surface Analytics, Trace Analytics and Chemometry
Technische Universität Wien (Vienna University of Technology).

Vienna, 07.12.2022

(David Ken Gibbs)

Affidavit

I declare in lieu of oath, that I wrote this thesis and preformed the associated research myself, using only literature cited in this work. If text passages from sources are used literally, they are marked as such.

I confirm that this work is original and has not been submitted elsewhere for any examination, nor is it currently under consideration for a thesis elsewhere. This thesis is identical to the version examined by the reviewers.

(David Ken Gibbs)

Eidesstaatliche Erklärung

Ich erkläre an Eides statt, dass die vorliegende Arbeit nach den anerkannten Grundsätzen für wissenschaftliche Abhandlungen von mir selbstständig erstellt wurde. Alle verwendeten Hilfsmittel, insbesondere die zugrunde gelegte Literatur, sind in dieser Arbeit genannt und aufgelistet. Die aus den Quellen wörtlich entnommenen Stellen, sind als solche kenntlich gemacht.

Das Thema dieser Arbeit wurde von mir bisher weder im In- noch Ausland einer Beurteilerin/einem Beurteiler zur Begutachtung in irgendeiner Form als Prüfungsarbeit vorgelegt. Diese Arbeit stimmt mit der von den Begutachterinnen/Begutachtern beurteilten Arbeit überein.

(David Ken Gibbs)

Die approbierte gedruckte Originalversion dieser Diplomarbeit ist an der TU Wien Bibliothek verfügbar
The approved original version of this thesis is available in print at TU Wien Bibliothek.
TU Bibliothek Your knowledge hub WIEN

Abstract

Polymers are a class of substances employed in a variety of fields, considering that their structural and mechanical properties can be fine-tuned for the desired application. When mechanical, thermal and chemical stability are required, high-performance polymers are employed, which in their application setting can be subject to moisture that degrades the polymers. Hence, water absorption by polymers – in particular thin polymer films – is of high technological interest, specifically for the semiconductor and microelectronics industry.

For material characterization, water absorption is mostly analyzed gravimetrically or by titration, but the employed methods are either indirect or require large sample quantities. The presented work aims to realize the analysis of water absorption by means of Laser Ablation-Inductively Coupled Plasma-Mass Spectrometry (LA-ICP-MS) as a semi-non-destructive technique for the direct, elemental analysis of hydrogen. Deuterium analysis via ICP-MS was recently achieved for mixtures of regular water and deuterium oxide by detecting the polyatomic ion $^{40}Ar^{2}D^{+}$, which is formed in the ICP plasma through collision. However, analyzing solids via LA-ICP-MS based on the $^{40}Ar^{2}D^{+}$ ion is a novelty. A major advantage of Laser Ablation as sample introduction method compared to liquid ICP-MS is the enhanced rate of sample introduction, reducing wash-out times by orders of magnitude. Additionally, the sample does not have to be transformed into a liquid; hence, sample consumption and contamination are decreased, whilst spatial information is obtainable too.

Transfer to Laser Ablation is accomplished by spiking polymer matrices with benzoic acid-2,3,4,5,6-d_5 so as to prepare standards with defined amounts of added deuterium. Two types of solid standards are prepared: pellets and polymer films, where the pellets are mainly used for method development. Both ultimately allow for the quantification of deuterium, but only the film standards are investigated more thoroughly as they match the matrix of the desired application example to a greater extent. For instance, ablation in helium and argon atmosphere are compared and internal standardization approaches discussed. The optimized LA-ICP-MS parameters allow for calibration of deuterium in a region of 0-10 $mg \cdot g^{-1}$, where four standards with 5 $mg \cdot g^{-1}$ exhibit a relative standard deviation of 7-10 % (based on nine repeat measurements each). In principle, the calibration of the film standards facilitates the analysis of water absorption within 0-50 mg per gramme of polymer, when respecting the stoichiometric factor of deuterium in deuterium oxide.

Die approbierte gedruckte Originalversion dieser Diplomarbeit ist an der TU Wien Bibliothek verfügbar
The approved original version of this thesis is available in print at TU Wien Bibliothek.

Water absorption of three industrial polyimide types is analyzed by subjecting samples to deuterium oxide in liquid form. First, samples were frozen to -18 °C in order to trap the water in the polymer. Then, the samples are ablated in a cooling stage, considering that water desorbs from the surface due to the dry ablation gas, creating a comparatively large background at the mass corresponding to the $^{40}Ar^{2}D^{+}$ ion. The in-house produced cooling stage is operated at -12 °C, thus reducing the background and enabling the detection of differences in water uptake between the polyimide types.

The results of this thesis provide a foundation for further research on water absorption by polymers via LA-ICP-MS. The ability of Laser Ablation to obtain spatial resolution, i.e., the possibility to perform depth profiling/imaging, is a key benefit that makes the presented method a promising candidate to analyze local differences in polymer degradation caused by water absorbed by the matrix.

Die approbierte gedruckte Originalversion dieser Diplomarbeit ist an der TU Wien Bibliothek verfügbar
The approved original version of this thesis is available in print at TU Wien Bibliothek.
TU Bibliothek Your knowledge hub WIEN

Kurzfassung

Polymere sind eine Verbindungsklasse, die in vielen verschiedenen Gebieten genutzt wird, da ihre strukturellen und mechanischen Eigenschaften für die jeweilige Anwendung zugeschnitten werden können. Sind mechanische, thermische und chemische Stabilität vonnöten, werden Hochleistungspolymere eingesetzt, die in ihrem Einsatzgebiet (Luft-)Feuchte ausgesetzt sind und durch diese degradiert werden. Deshalb ist die Wasseraufnahme durch Polymere, insbesondere durch Dünnfilme, von großer Bedeutung, vor Allem in der Halbleiterindustrie und Mikroelektronik.

Im Hinblick auf Materialcharakterisierung wird Wasserabsorption üblicherweise gravimetrisch oder über Titration bestimmt, jedoch sind die Methoden entweder indirekt oder benötigen große Probenvolumen. Ziel dieser Arbeit ist die Analyse von Wasserabsorption durch Laser Ablation-Inductively Coupled Plasma-Mass Spectrometry (LA-ICP-MS) als quasi-zerstörungsfreies, direkte Elementaranalyseverfahren für Wasserstoff. Die Messung von Deuterium mit ICP-MS wurde kürzlich für Mischungen aus normalem Wasser und Deuteriumoxid durchgeführt, indem das polyatomare Ion $^{40}Ar^{2}D^{+}$ detektiert wurde, welches sich im ICP durch Kollision bildet. Feste Proben mittels LA-ICP-MS zu analysieren ist hingegen eine Neuheit. Ein wesentlicher Vorteil von Laser Ablation im Vergleich zur Einbringung flüssiger Proben ist die höhere Flussrate des Trägergases, was die Auswaschzeit um Größenordnungen verringert. Darüber hinaus müssen Proben nicht zuerst in eine Flüssigkeit transformiert werden, weshalb Probenverbrauch sowie -kontamination verringert werden und zusätzlich Informationen über die räumliche Verteilung des Analyten in der Probe zugänglich sind.

Der Transfer zu Laser Ablation wird durch das Hinzufügen von Benzoesäure-2,3,4,5,6-d_5 zu Polymermatrices ermöglicht, um Standards mit definiertem Deuteriumgehalt zu erstellen. Zwei Arten von Standards werden hergestellt: Presslinge und Polymerfilme, wobei erstere für die Methodenentwicklung verwendet werden. Alles in Allem ermöglichen beide die Quantifizierung von Deuterium, aber die Polymerfilme werden gründlicher untersucht, da sie der gewünschten Anwendung in Bezug auf die Matrix stärker ähneln. Im Zuge dessen werden bspw. Helium und Argon als Ablationsatmosphäre verglichen und Methoden zur internen Standardisierung diskutiert. Die optimierten LA-ICP-MS Parameter ermöglichen die Kalibration von Deuterium zwischen 0 und10 $mg \cdot g^{-1}$, wobei vier Standards mit 5 $mg \cdot g^{-1}$ eine relative Standardabweichung von 7-10 % aufweisen (basierend auf neun

Die approbierte gedruckte Originalversion dieser Diplomarbeit ist an der TU Wien Bibliothek verfügbar
The approved original version of this thesis is available in print at TU Wien Bibliothek.
TU Bibliothek Your knowledge hub WIEN

Messungen eines Standards). Theoretisch erlaubt die Kalibration der Filmstandards folglich die Analyse der Wasserabsorption in einem Bereich von 0-50 mg pro Gramm Polymer (bei Berücksichtigung des stöchiometrischen Faktors von Deuterium in Deuteriumoxid).

Die Wasseraufnahme von drei industriellen Polyimidfilmen wird durch Einlegen der Proben in Deuteriumoxid getestet. Zuerst müssen die Proben dafür eingefroren werden (-18 °C), um das Wasser im Polymer festzuhalten. Für die Ablation ist die Kühlung der Proben in einer sogenannten Cryostage notwendig, da das Wasser aufgrund der trockenen Ablationsatmosphäre von der Probe desorbiert, was zu einem hohen Untergrund auf der Masse des $^{40}Ar^{2}D^{+}$-Ions führt. Die verwendete Cryostage wurde intern produziert und wird bei -12 °C betrieben, was den Untergrund merklich reduziert und dadurch Unterschiede im Wasseraufnahmeverhalten zwischen den verschiedenen Polyimidtypen ersichtlich macht.

Ausgehend von dieser Arbeit sind weitere LA-ICP-MS Untersuchungen bezüglich der Wasserabsorption von Polymeren möglich. Die Tatsache, dass Laser Ablation räumliche Auflösung ermöglicht, d.h. Tiefenprofile oder Imaging zugänglich sind, ist ein entscheidender Vorteil der entwickelten Methode. Deshalb werden zukünftig Anwendungen angestrebt, wo lokale Unterschiede im Degradationsverhalten von Polymeren von Interesse ist, welche durch von der Matrix absorbiertes Wasser verursacht werden.

Die approbierte gedruckte Originalversion dieser Diplomarbeit ist an der TU Wien Bibliothek verfügbar
The approved original version of this thesis is available in print at TU Wien Bibliothek.
TU Bibliothek Your knowledge hub WIEN

Danksagung

An dieser Stelle möchte ich eine Seite Text dafür verwenden, denen zu danken, die mir die Diplomarbeit selbst, aber auch den Weg dorthin ermöglicht haben, und zwar in ungefähr umgekehrt chronologischer Reihenfolge des Kennenlernens. Bezüglich Ersterem gilt mein Dank natürlich zu allererst meinem Betreuer Andreas. Vielen Dank, dass du mich zuerst als Wahlpraktikant und jetzt als Diplomand in deine Arbeitsgruppe aufgenommen hast. Danke für die Zeit, die du mir – gerade in der Endphase – geopfert hast. Aber natürlich auch für die aufbauenden Worte, dein stets offenes Ohr und deine Unterstützung. Großer Dank geht auch an die gesamte Arbeitsgruppe, insbesondere an die Lukas sowie DissertantInnen Birgit, Jakob und Max für die fachliche und praktische Unterstützung. Besonders erwähnen möchte ich noch Tobias und Laura, die mir während der Zeit am Institut abgesehen von den praktischen Aspekten vor allem auch eine emotionale Stütze waren – danke dafür.

Danken möchte ich hier auch meinen StudienkollegInnen, die mich seit dem Bachelor bereits begleiten und insbesondere zu dieser Zeit viele Stunden am Campus mit mir verbracht haben. Danke an Tobi, Jakob und Michi für die vielen Gespräche in Momenten, wo ich jemanden zum Reden brauchte. Eine Person will ich an dieser Stelle noch hervorheben: danke für Alles, Glix. Es bedeutet mir sehr viel, dass wir schon einiges zusammen gemacht haben, und ich hoffe, dass das auch in der Zukunft so bleibt.

Auch wenn wir uns nicht mehr so häufig sehen, bleibt Joni eine der wichtigsten Personen in meinem Leben. Ohne ihn wäre die Schulzeit nicht dieselbe gewesen und vielleicht wäre ich heute auch nicht hier (gelandet). Der Union Hypo Vöcklabruck, insbesondere Hary, möchte ich an dieser Stelle für die vielen Jahre im Handballsport danken.

Zu guter Erst, danke an meine Familie. Danke Oma, danke Christoph, danke Doris. Danke für Alles, was ihr für mich getan habt und immer noch tut, auch wenn ich nur mehr selten da bin. Thank you for everything, Dad. I can only imagine how hard it is to have your child grow up in a different country, but I know you did your best.

Und danke Mama, danke, danke, danke. Du musstest so viel aufgeben, um mich großzuziehen. Auch wenn ich kein schwieriges Kind war, gab es doch viele Probleme, die dir etliche schlaflose Nächte bereitet haben. Ich könnte mir keine bessere Mutter wünschen. Von ganzem Herzen: ich hab‘ dich lieb, auch wenn ich es selten sage.

Die approbierte gedruckte Originalversion dieser Diplomarbeit ist an der TU Wien Bibliothek verfügbar
The approved original version of this thesis is available in print at TU Wien Bibliothek.
TU Bibliothek Your knowledge hub WIEN

Contents

Die approbierte gedruckte Originalversion dieser Diplomarbeit ist an der TU Wien Bibliothek verfügbar
The approved original version of this thesis is available in print at TU Wien Bibliothek.

Die approbierte gedruckte Originalversion dieser Diplomarbeit ist an der TU Wien Bibliothek verfügbar
The approved original version of this thesis is available in print at TU Wien Bibliothek.

List of Figures

Die approbierte gedruckte Originalversion dieser Diplomarbeit ist an der TU Wien Bibliothek verfügbar
The approved original version of this thesis is available in print at TU Wien Bibliothek.

Die approbierte gedruckte Originalversion dieser Diplomarbeit ist an der TU Wien Bibliothek verfügbar
The approved original version of this thesis is available in print at TU Wien Bibliothek.

List of Tables

Die approbierte gedruckte Originalversion dieser Diplomarbeit ist an der TU Wien Bibliothek verfügbar
The approved original version of this thesis is available in print at TU Wien Bibliothek.

List of Abbreviations

Abbreviation	Description
^{2}D	Deuterium isotope of hydrogen
$^{40}Ar^{2}D^{+}$	Polyatomic species consisting of ^{40}Ar and ^{2}D
deuterated benzoic acid	Benzoic acid-2,3,4,5,6-d5
ICP	Inductively Coupled Plasma
ICP-MS	ICP-Mass Spectrometry
LA-ICP-MS	Laser Ablation-ICP-MS
LIBS	Laser Induced Breakdown Spectroscopy
LIBS J200	Laser system with a wavelength of 266 nm
m/z	Mass-to-charge ratio
Nd:YAG	Neodymium-doped yttrium aluminum garnet
NMP	N-Methyl-2-pyrrolidone
NWR213	Laser system with a wavelength of 213 nm
PI 1 , PI 2, PI 3	Investigated industrial polyimide films
PMMA	Poly(methyl methacrylate)
polyimide	Commercial polyimide P84 powder
Pt-acac	Platinum(II) bis(acetylacetonate)
RSD	Relative standard deviation (expressed in percent)
SBR	Signal-to-background ratio
SN	Solution nebulization

Die approbierte gedruckte Originalversion dieser Diplomarbeit ist an der TU Wien Bibliothek verfügbar
The approved original version of this thesis is available in print at TU Wien Bibliothek.

1. Introduction

Polymers possess a large variety of properties and are found in more and more life situations. Natural polymers, such as proteins or nucleic acids, as well as synthetic polymers, e.g., polyesters or polyethylene, both consist of large molecules created by the polymerization of small molecules, i.e., the monomers. The majority of synthetic polymers are often condemned by the general public as environmentally harmful because of their limited recyclability and high carbon footprint, but in many applications they are irreplaceable. The wide array of materials and the ability to fine-tune their properties makes polymers the ideal candidate for the use in high-performance settings, where they are subjected to harsh conditions, such as humidity, thermal stress, mechanical stress and challenging chemical environments, among others [1,2].

Absorption of water by polymers in the form of humidity, that is, from the ambient atmosphere, or in terms of uptake from a liquid environment can be beneficial or detrimental, depending on the context. “The moisture content of a plastic is very intimately related to such properties as electrical insulation resistance, dielectric losses, mechanical strength, appearance, and dimensions“ [3]. Nafion™, a synthetic polymer with ionic properties based on perfluorinated sulfonic acid, has drawn attention for its proton conducting capability and is used as the membrane in proton exchange membrane fuel cells (PEMFC) [4]. Water and proton transport are highly correlated owing to several interactions between proton and solute; a higher water content leads to an increased dielectric constant and as a result improved conductivity [4,5]. Conversely, swelling of the ionomer can cause mechanical stresses, resulting in failure of the membrane [6]. Thin polymer films are also utilized in microelectronics as a matrix for nanocomposite layers, for example. These layers act as barrier coatings or encapsulation materials preventing moisture and gases corroding the electronics [7]. Again, swelling of these polymeric layers can induce mechanical stresses or increased permittivity of corroding agents, ultimately causing fatigue of the component.

Consequently, it is apparent that the uptake of water by polymeric materials is of technological interest. For material characterization, this property is mostly determined gravimetrically as set out in DIN EN ISO 62:2008-05 ([8]) or the technically equivalent ASTM D570-98(2010)e1 ([9]). Simply put, a sample is heated in an oven, weighed, subjected to humidity or submerged in water and finally weighed again. However, these standards are not applicable for thin polymer films; ASTM D570-98(2010)e1 sets the lower

Die approbierte gedruckte Originalversion dieser Diplomarbeit ist an der TU Wien Bibliothek verfügbar
The approved original version of this thesis is available in print at TU Wien Bibliothek.

limit for sheet thickness at 0.13 mm [9]. Other gravimetric methods include techniques such as thermogravimetric analysis (TGA), differential thermogravimetry (DTG) and electrothermal analysis (ETA) [10]. The main drawback of gravimetry is the fact that soluble components may be extracted by the water and that volatiles can be lost during heating of the sample, both of which cause inaccuracies. Coulometric methods based on Karl Fischer titration and manometric analyses are described in DIN EN ISO 15512:2019-09 ([11]), but are by and large limited to sample amounts of more than 0.1 g.

Furthermore, infrared spectroscopy can also provide information on the interaction between polymer and water with high sensitivity. Overtone and combination bands that lie in the near infrared region (14,300-5,000 cm^{-1}) are specific for water and hold the desired quantitative information. For the direct analysis of solids, attenuated total reflection (ATR) can be employed, but is limited by a penetration depth in the low µm range. Another non-destructive, spectroscopic method is wide-line nuclear magnetic resonance. The line width of protons tends to scale with their mobility, which is why protons originating from water adsorbed on solids can be differentiated from the protons belonging to the polymer. Furthermore, since polymers show dielectric properties, indirect methods based on the measurement of conductivity, impedance etc. are possible. [10]

Most of the aforementioned techniques are indirect, meaning that the analyte species is not the water itself; for instance, gravimetry analyzes the weight change of a sample. In contrast, the aim of this thesis is to directly analyze the hydrogen as an elemental species so as to investigate the feasibility of water uptake determination by means of Laser Ablation-Inductively Coupled Plasma-Mass Spectrometry (LA-ICP-MS). A more detailed overview of Laser Ablation (LA) and Inductively Coupled Plasma-Mass Spectrometry (ICP-MS) is given in the theoretical section, but in principle, the fundamental processes of signal generation are as follows: production of an aerosol by ablation of the sample in a gas atmosphere; transport of the aerosol to the Inductively Coupled Plasma (ICP); vaporization, atomization and (partial) ionization of the aerosol by the ICP; sampling of the plasma and extraction of ions; separation of the ions according to their mass-to-charge ratio in a mass analyzer; signal enhancement and detection [12,13]. In contrast to the techniques described previously, LA-ICP-MS also provides access to spatial resolution. If the laser is scanned across the sample surface and the recorded intensity is plotted, a two-dimensional image is generated; if the laser is held in place and ablates the sample multiple times, a depth profile is created.

Die approbierte gedruckte Originalversion dieser Diplomarbeit ist an der TU Wien Bibliothek verfügbar
The approved original version of this thesis is available in print at TU Wien Bibliothek.
TU Bibliothek Your knowledge hub WIEN

In order to determine their water absorption, the polymer samples are submerged in water in analogy to the gravimetric methods discussed earlier. If this was performed using regular, that is, deionized water, there would be no possible way to distinguish between the hydrogen ions from the absorbed water and those from the polymer. Therefore, so-called heavy water is employed instead, which is rich in deuterium (^{2}H, denoted ^{2}D in the following). Deuterium is one of the two stable hydrogen isotopes – the other one being protium – and consists of one proton, one neutron and one electron. The ratio of deuterium and protium (^{2}D/^{1}H) on earth is often referenced as $(155.76 \pm 0.05) \cdot 10^{-6}$, a value based on measurements of the isotopic standard Vienna Standard Mean Ocean Water (VSMOW) [14]. On the other hand, heavy water is usually deuterium-enriched in excess of 99 %, inverting the ^{2}D/^{1}H ratio. Therefore, the vast majority of deuterium detected from a polymer sample subjected to heavy water will originate from the heavy water itself.

In spite of the rather straightforward concept, the analysis of hydrogen isotopes by ICP-MS is a novel approach. Low-mass ions suffer greatly from so-called space-charge effects: same sign ions repel each other, hence defocusing the beam of ions travelling from the ICP to the mass analyzer, e.g., a quadrupole [12,13]. Because of their low kinetic energy, low-mass ions are affected more heavily and are either driven towards the edges of the ion beam or lost entirely; for a more detailed explanation, cf. [12]. Combined with other collisional effects, this is the reason why the transmission of low-mass ions is significantly lower than for higher masses in commercial ICP-MS instruments [12]. Besides, hydrogen is not as readily ionized in the argon-based ICP plasma compared to other analytes [15]. The degree of ionization is determined by the Saha equation, where the ionization potential of the analyte – 13.6 eV in the case of hydrogen – relative to that of argon (15.76 eV) is a major factor. For plasmas of identical temperature, higher differences in ionization potential result in higher degrees of ionization. As a consequence, less hydrogen ions are produced than, for example, chromium ions (ionization potential of 6.76 eV) from the same amount of atoms. Furthermore, it is important to note that most commercial instruments usually only allow for the analysis of masses higher than 4, which makes hydrogen as analyte inaccessible [15].

Galbács et al. ([15]) realized that polyatomic ions can act to bypass this issue. Polyatomic ions are a type of spectral interference in mass spectrometry, where ions combine to molecular ions in the plasma through reaction after colliding with each other. This is usually an unwanted process; for instance, $^{40}Ar^{16}O^+$ – formed by reaction of ubiquitous argon ions with residual oxygen species – interferes with $^{56}Fe^+$, the most common stable isotope

Die approbierte gedruckte Originalversion dieser Diplomarbeit ist an der TU Wien Bibliothek verfügbar
The approved original version of this thesis is available in print at TU Wien Bibliothek.
TU Bibliothek Your knowledge hub WIEN

of iron, and impairs the quantification thereof. However, the formation of polyatomic ions can be exploited too, as is the case for the method of deuterium quantification proposed by Galbács et al. [15]. Based on their thermodynamic modelling of the ICP plasma and subsequent experiments, the molecular ion $^{40}Ar^{2}D^{+}$ is produced in sufficient amounts such that quantification of deuterium in mixtures of deuterium-depleted and deuterium-enriched water is possible [15]. Despite not addressing the low degree of ionization for hydrogen, the shift of mass improves the ion transmission and therefore enhances the signal. However, this notion disregards the efficiency of formation of the molecular ion in the plasma.

Likewise, $^{40}Ar^{2}D^{+}$ is the foundation for this thesis. To the best knowledge of the author, applying LA-ICP-MS for the measurement of deuterium in solids is a novelty. The assumption is that the type of sample injection is inconsequential, as long as enough deuterium atoms are transported to the ICP, thus LA-ICP-MS should too have qualitative and quantitative capabilities. Based on the data provided, Galbács et al. required large amounts of time to achieve signal stability and wash-out of samples, both of which should be reduced by laser ablation. This comes as no surprise since the flow rate in liquid injection ICP-MS is in the order of $\mu L \cdot min^{-1}$, whereas in laser ablation the flow rate of the carrier gas is usually hundreds of $mL \cdot min^{-1}$. Hence, the analyte transport is considerably faster and less signal broadening is expected for laser ablation, while analysis time is decreased too. In the following work, the viability of LA-ICP-MS measurement of deuterium is investigated in terms of obtainable qualitative and quantitative information.

First, standards with known quantities of deuterium were produced by adding benzoic acid-2,3,4,5,6-d_5 to a polymer matrix, showing that even quantification of deuterium in solids is possible. Secondly, deuterium is introduced into polymer samples by submersion into heavy water; this shall serve as an application example. Since the vast majority of the hydrogen in the polymer is naturally protium, measuring the deuterium signal – introduced in the shape of deuterium oxide – enables drawing conclusions on water absorption by the polymer. After elaborating on the theoretical background of laser ablation and ICP-MS, the sample and standard preparation, instrumentation as well as methodology are explained, before results are discussed and an outlook is given.

Die approbierte gedruckte Originalversion dieser Diplomarbeit ist an der TU Wien Bibliothek verfügbar
The approved original version of this thesis is available in print at TU Wien Bibliothek.

2. Theoretical Background

The aim of the following sections is to give an overview of the basic principles of Laser Ablation (LA) and Inductively Coupled Plasma Mass Spectrometry as well as the hyphenation of the two techniques. However, the main focus shall lie on topics relevant to this thesis and the equipment used therein. Hence, lasers of the neodymium-doped yttrium aluminum garnet (Nd:YAG) type and the interaction of laser energy with solids are discussed in terms of LA, whilst quadrupole mass filters will be the center of attention with regards to ICP-MS.

2.1 Laser Ablation (LA)

Absorption of energy in the shape of photons can lead to the ablation of a solid. If this is achieved using a focused, pulsed laser beam with sufficient energy, this process is called laser ablation [16]. During the absorption, parts of the solid are removed "by melting, fusion, sublimation, ionization, erosion and/or explosion", producing vaporized solid, a plasma in the vicinity of the location of incidence as well as fine particles [17]. The interaction of the vapor with the induced plasma is the foundation of Laser Induced Breakdown Spectroscopy (LIBS). Alternatively, vapor and particles can be transferred to a hyphenated measurement system such as an ICP-MS instrument.

2.1.1 Interaction of Lasers with Condensed Matter

In essence, laser ablation is "the conversion of an initial electronic or vibrational photo-excitation into kinetic energy of nuclear motion, leading to the ejection of atoms, ions, molecules, and even clusters from a surface." [18] Laser ablation can be seen as a sputtering process, in which more than one tenth of a microlayer of sample is removed from the surface per pulse. During this process, the laser transfers its energy to the surface down to a penetration depth characteristic for its wavelength, usually limited to a near-surface region of 0.02-5 µm. As a consequence, the excitation of free electrons and electronic or vibrational transitions in atoms, ions, molecules or optically active defects may occur. The electronic structure, composition, topography and defect population of the irradiated surface as well as laser wavelength and pulse duration are key factors influencing mechanism, density and lifetime of the resulting excitation. Besides, the inherent surface modifications are subject to surface morphology and roughening as well as the ambient atmosphere. [13,18]

More generally, the ablation process can be divided into three sections: "bond breaking and plasma ignition, plasma expansion and cooling, and particle ejection and condensation". [17] While particle condensation occurs at 10^{-3} s after the laser pulse is

Die approbierte gedruckte Originalversion dieser Diplomarbeit ist an der TU Wien Bibliothek verfügbar
The approved original version of this thesis is available in print at TU Wien Bibliothek.
TU Bibliothek Your knowledge hub WIEN

completed, electronic absorption of laser energy takes place after 10^{-15} s, hence making the ablation processes span several order of magnitude in time. [17]

Laser pulse duration and irradiance can determine, which bond-breaking mechanism dominates during plasma ignition. Coulomb explosions govern the process for high irradiances $>10^{13}$ W·cm^{-2} and fs pulse durations. For ps pulses, both thermal and/or non-thermal mechanisms can lead to melting, depending on laser irradiance. Thermal vaporization processes such as melting, fusion, sublimation, vaporization, etc. dominate for irradiances $<10^{8}$ W·cm^{-2} and ns pulses. With ns pulses, plasma shielding can occur, i.e., the end of the pulse is absorbed by the plasma, directly affecting the amount of vapor formed from the solid. This is pictured schematically in Figure 1 and is a result of increased amounts of inverse Bremsstrahlung, where "free electrons gain kinetic energy from the laser beam and collisions among sample atoms and ions, electrons, and gas species". [17] The energy of the plasma can also increase due to the additional heating. [16,17,19]

Plasma expansion is an adiabatic process (until ~1 µs after the pulse) and is highly dependent on the expansion medium, i.e., the ambient atmosphere, and the initial plasma properties at the end of the pulse (electron number density, temperature and expansion speed), which in turn strongly depend on the laser properties. In a gas environment, the ejecta produce shockwaves upon compressing the surrounding media. Furthermore, the plasma plume is a mixture of atoms, ions and mass from the sample and the ambient atmosphere, which is not the case in a vacuum. [17]

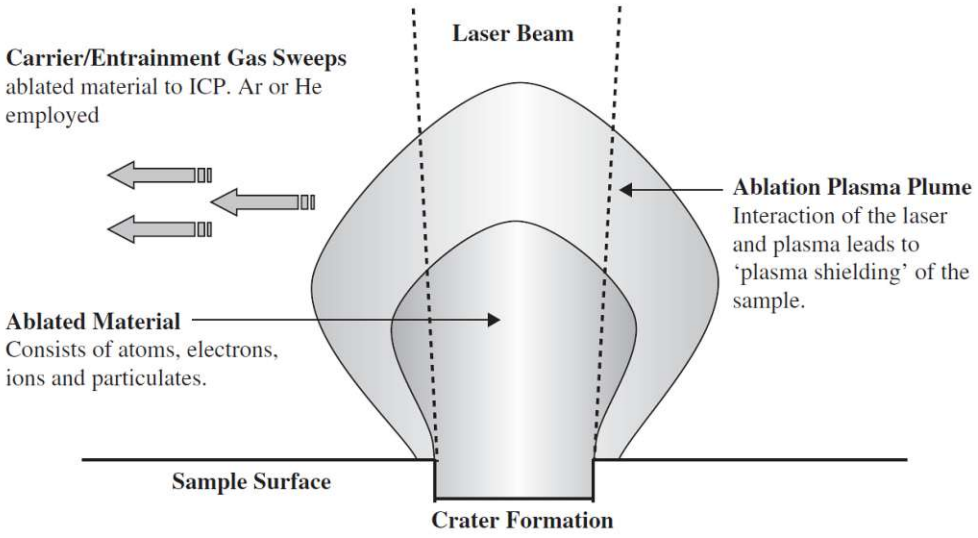

Figure 1: Laser ablation plume – consisting of hot atoms, ions molecules and particles – in the context of LA-ICP-MS. Plasma shielding reduces the amount of ablated mass [13].

Die approbierte gedruckte Originalversion dieser Diplomarbeit ist an der TU Wien Bibliothek verfügbar
The approved original version of this thesis is available in print at TU Wien Bibliothek.

In the particle formation step, the vapor produced in the bond-breaking phase condenses to nano-sized particles, contingent upon the boiling temperature of the material. The particle size depends on the density of the vapor plume and cooling time. Alternatively, particles may also be ejected from the molten surface by means of explosive boiling, which is common for ns pulse lasers. Heating rates of 10^{12} °C·s^{-1} are reported, resulting in a melt, which spreads into the bulk during the pulse. High-pressure bubbles form and expand rapidly, succeeded by molten droplets being violently ejected from the surface due to the pressure gradients. A further ejection mechanism is also related to the high heating rates, namely solid sample exfoliation. In this process, the high thermal stress gradients break the sample into irregular-shaped particles (in contrast to condensed vapor) leading to particle ejection. For LA-ICP-MS conditions, vapor condensation is seen as the dominant particle generation mechanism. [17,19]

Apart from laser pulse duration and irradiance, the laser wavelength also influences the ablation mechanism. Shorter wavelengths lead to higher energies for bond-breaking and ionization. When the bond energy is exceeded, the incident photons can ionize the surface and non-thermal processes dominate so that the ablation rate, i.e., the amount of ablated mass per laser pulse per unit area, increases. Larger wavelengths lead to an increase in inverse Bremsstrahlung, hence more plasma shielding and less ablated mass. Additionally, elemental fractionation increases; for LA-ICP-MS, elemental fractionation describes non-stoichiometric effects during ablation, transport and atomization/ionization in the ICP plasma that affect the generated signal. For instance, micrometer-sized particles formed during ablation have been found to evaporate in an insufficient manner leading to spikes and drifts in the resulting data. However, there are several more processes, which fall under the rather general term of elemental fractionation. [12,13,17,19,20]

2.1.2 Laser System

Solid state lasers, in particular Nd:YAG lasers with ns pulses (5-10 ns) and wavelengths down to 213 nm, have been used extensively for LA-ICP-MS as a result of low maintenance costs, compact size and easy handling. [12,19,21] In principle, optical activity is achieved within the otherwise transparent host material $Y_3Al_5O_{12}$ by doping with Nd, whose trivalent ions partially replace Y^{3+} sites, yielding a pale purple crystal.

A simplified energy scheme is shown in Figure 2a). First, optical pumping occurs, where the light from a flash lamp or a suitable laser source is absorbed by the active medium,

Die approbierte gedruckte Originalversion dieser Diplomarbeit ist an der TU Wien Bibliothek verfügbar
The approved original version of this thesis is available in print at TU Wien Bibliothek.

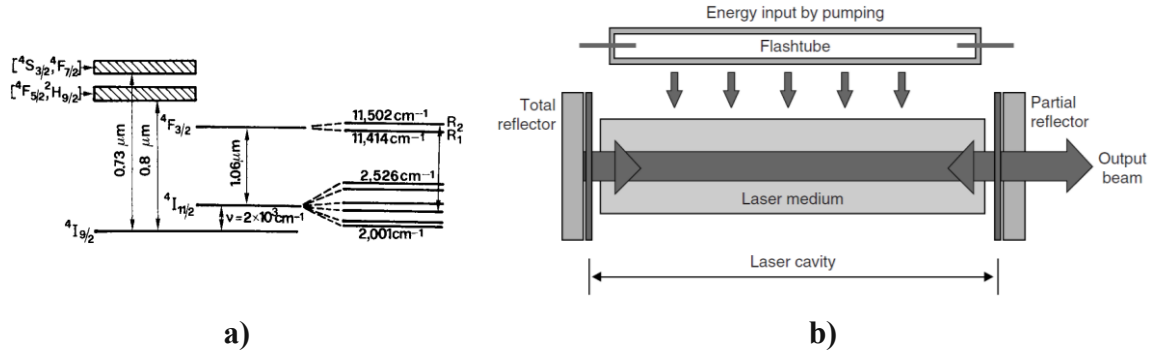

Figure 2: a) Simplified energy scheme for the Nd:YAG laser [22]. The most prominent laser emission with a wavelength of 1064 nm occurs for the transition $^4F_{3/2} \rightarrow {}^4I_{11/2}$. b) Principal structure of a laser, composed of a pumping mechanism (flashtube), the laser medium and a resonator (total and partial reflector) [12].

exciting atoms into the pumping level, e.g., $^4F_{5/2}$. From there, a fast nonradiative decay to the metastable $^4F_{3/2}$ level occurs. Without going into further detail, the strongest laser transition is that from the level $^4F_{3/2}$ to $^4I_{11/2}$ with a wavelength of 1064 nm. A fast nonradiative decay from $^4I_{11/2}$ to $^4I_{9/2}$ ensures that thermal equilibration between those states is achieved rapidly. As the energy difference between $^4I_{11/2}$ and $^4I_{9/2}$ is significantly larger than kT, the $^4I_{11/2}$ level can be considered constantly empty according to Boltzmann statistics. Hence, this transition scheme can be seen as a four level laser operation scheme. Considering that the transitions $^4F_{5/2} \rightarrow {}^4F_{3/2}$ and $^4I_{11/2} \rightarrow {}^4I_{9/2}$ are rapid (within the ns range) and pumping guarantees the transition to the upper laser level, population inversion is achieved, i.e., the upper level ($^4F_{3/2}$) has a higher population than the lower level ($^4I_{11/2}$). [12,22]

In principle, a Nd:YAG laser consists of the three elements shown in Figure 2b): a pumping mechanism (flash light or laser), the optically active laser medium and a resonator structure, represented by two reflectors (i.e., mirrors). Photons emitted by the laser medium, which are emitted along the axis of the laser cavity, are reflected by the mirrors multiple times and can interact with other excited atoms. Therefore, stimulated emission arises and an amplification each time a photon passes through the medium follows so that many photons with identical wavelength and phase are released. Through non-linear optics the fundamental wavelength of 1064 nm of the Nd:YAG laser can be frequency multiplied. As a consequence, the wavelength can be shifted from the near-infrared to the ultraviolet region, with (frequency quadrupled) 266 nm and (frequency quintupled) 213 nm systems being common for LA-ICP-MS. [12,19]

Another type of lasers used for LA-ICP-MS are excimer lasers, whose principle of photon generation differ significantly from Nd:YAG lasers. An excimer is defined as a molecule consisting of two monomers, which cannot bond together in the ground state (due

Die approbierte gedruckte Originalversion dieser Diplomarbeit ist an der TU Wien Bibliothek verfügbar
The approved original version of this thesis is available in print at TU Wien Bibliothek.
TU Bibliothek Your knowledge hub WIEN

to repulsion), but in the excited state possess a minimum on the potential energy curve for a dimeric species. The excited dimer decays to the ground state by emitting characteristic radiation in the near-ultraviolet region, whilst the dimer itself decomposes, yielding the monomers. As this emission can also be stimulated in all molecules by the photon emitted in the decay of one dimer, laser operation is achieved. The maintenance costs are higher than for Nd:YAG lasers, but the energy output range is higher. Moreover, excimer lasers produce flat-top beam profiles as opposed to Gaussian profiles obtained with Nd:YAG lasers, which ensures more consistent and defined ablation patterns. [12,19,23]

2.2 Inductively Coupled Plasma Mass Spectrometry (ICP-MS)

ICP-MS is a routine analysis method for a wide array of applications in inorganic trace- and ultra-trace analysis. Multi-element analysis of materials such as semiconductors, metals, alloys, ceramics and polymers – to name a few – can be performed with high sensitivity and with a large dynamic range, meaning that major and trace elements can be analyzed simultaneously. [23] ICP-MS instruments generally consist of the following components:

- sample introduction system: generation of an aerosol, which is then transported to the ICP; common techniques include solution nebulization (liquid sample injection), laser ablation and electrothermal vaporization
- ICP: ionization of the wet or dry aerosol (gas and analyte)
- interface between the atmospheric pressure region of the ICP and the high vacuum of the mass spectrometer
- ion optics: focusing of ions after transition to the high vacuum
- mass filter: separation of ions in the space or time domain according to their mass-to-charge (m/z) ratio
- detector.

These parts will be discussed further in the subsequent chapters, before turning the attention on spectral interferences and how they can be exploited for analysis.

2.2.1 Laser Ablation as Sample Introduction System for ICP-MS

A simplified view of a typical LA-ICP-MS setup is illustrated in Figure 3. The sample is placed in an ablation cell atop a movable stage, which allows for three-dimensional positioning, accompanied by microscope optics (the viewing system) to observe the sample. Gas-tightness of the cell, equipped with entry and exit for the carrier gas, has to be ensured to transport ablated material to the ICP-MS. The laser beam is directed onto the sample surface through a window transparent for the specific laser wavelength. By ablating the sample, an aerosol, consisting of analytes and the surrounding atmosphere, is formed.

Die approbierte gedruckte Originalversion dieser Diplomarbeit ist an der TU Wien Bibliothek verfügbar
The approved original version of this thesis is available in print at TU Wien Bibliothek.
TU Bibliothek Your knowledge hub WIEN

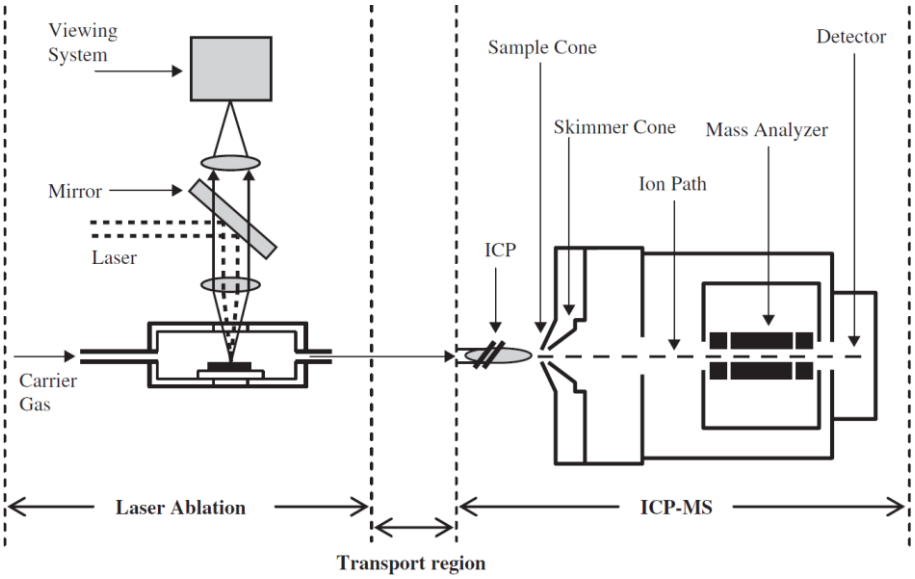

Figure 3: Scheme for the hyphenation of LA and ICP-MS [13]. By means of ablation, the sample is turned into an aerosol consisting of analyte particles and carrier gas; this aerosol is then transported to the ICP-MS.

Transport from the location of ablation to the ICP-MS is performed by the carrier gas, which also serves as the ablation atmosphere, with transport efficiencies as high as 90-100 % being reported recently, though they usually range from 10-60 % in most commercial setups. Different ablation atmospheres affect both ablation and transport. Traditionally, argon was used, but nowadays helium is routinely employed in LA-ICP-MS as the smaller particles produced during ablation are transported more efficiently towards the ICP and also vaporized more readily within the plasma. These effects are attributed to a lower density (greater transport efficiency), higher ionization energy (formation of smaller plasma) and higher thermal conductivity, all of which result in reduced condensational particulate growth. However, the particle size distribution produced during the ablation process – which can range from 2 nm to 5 µm – is not necessarily identical to that at the entrance of the ICP-MS due to condensation, vaporization or agglomeration during transport. Gravitational forces may result in large particles settling; vapor and small particle clusters may diffuse within the chamber and to the transfer tube. Logically, the connective tubing, that is, the inner diameter and length of the tubing, significantly influences transport efficiency. [12,13,19,20]

Most ICP-MS instruments used for routine analysis are equipped with a liquid sample introduction system. Hence, solid samples have to be converted into liquids via extraction or dissolution, which can introduce considerable amounts of contaminations or may not even be possible. In order to analyze the liquids they are transformed into an aerosol through nebulization and then pass through a spray chamber so as to filter out larger droplets, which would be desolvatized insufficiently in the plasma. Compared to the nebulization of

Die approbierte gedruckte Originalversion dieser Diplomarbeit ist an der TU Wien Bibliothek verfügbar
The approved original version of this thesis is available in print at TU Wien Bibliothek.
TU Bibliothek Your knowledge hub WIEN

liquid samples (referred to as solution nebulization), laser ablation has certain strengths and weaknesses, which are discussed as follows [20,21,24]:

Advantages:

- less standard preparation, resulting in decreased analysis time and reduced contamination induced by liquids in the sample preparation; furthermore, lower personal risks due to the chemicals used during sample preparation persist
- chemically inert elements and materials, e.g., samples that cannot be dissolved, can be analyzed
- reduced sample consumption (quasi-non-destructive method)
- enhanced sensitivity due to more efficient mass transport [13,19]
- spatially resolved sampling is accessible, i.e., imaging as well as depth profiles are possible

Disadvantages:

- like for solution nebulization, the use of internal standards is advisable in order to correct for changes in the ICP-MS instrument (e.g., cone conditions, vacuum pressure); additionally, variations in sample introduction, e.g., deviating mass ablation between replicate measurements, have to be compensated; however, selection of an internal standard is not trivial and may require extensive sample pretreatment
- complicated quantitation as a result of:
  - a lack of matrix-matching reference materials and established external calibration standards, which therefore are mostly produced in-house
  - no sample dilution being possible
  - typical calibration approaches common for aqueous solutions, e.g., single standard addition or isotope dilution, being impractical for solids
- the sample position in the ablation cell and laser focusing can lead to sensitivity shifts
- elemental fractionation (cf. 2.1.1, for further reading: [12,13,19,20]).

The fact that spatial resolution is possible with laser ablation is one of the major benefits of the technique compared to solution nebulization since the latter only provides bulk information. On the contrary, the more challenging quantification – at times requiring extensive method development – as well as elemental fractionation are notable drawbacks.

2.2.2 Inductively Coupled Plasma (ICP)

For the purpose of analyzing the injected sample aerosol with a mass spectrometer, the analytes have to be ionized first, which is accomplished by an inductively coupled plasma. With regards to the use as an ion source, an ICP is usually generated within a quartz torch comprising of three concentric tubes, a schematic of which is depicted in Figure 4. The inner tube (injector) guides the sample aerosol; the intermediate (auxiliary/tangential gas) and outer tubes (cool gas) provide the gas flow necessary for the formation and cooling of the

Die approbierte gedruckte Originalversion dieser Diplomarbeit ist an der TU Wien Bibliothek verfügbar
The approved original version of this thesis is available in print at TU Wien Bibliothek.
TU Bibliothek Your knowledge hub WIEN

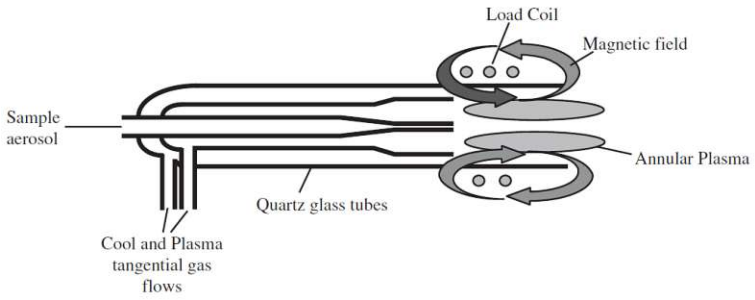

Figure 4: ICP torch [13]. Analytes enter in the shape of an aerosol and are desolvated, vaporized, atomized and (partially) ionized by the ICP. The plasma itself is maintained by the radio frequency power applied to the copper coil and argon gas flows.

plasma, respectively. If argon gas is subjected to the high-voltage discharge of a Tesla coil, some argon atoms are stripped of electrons. As a result of the application of a radio frequency power of 750-1700 W to a copper coil positioned at the front of the torch, an alternating current is established. The oscillations of this current (with a frequency in the MHz range) bring about electrical and magnetic fields at the top of the torch, with the latter trapping the electrons generated by the initial spark, accelerating them in closed circular paths. Collisions of neutral argon atoms with the electrons ionizes the atoms (hence, more electrons are produced), establishing a chain reaction. These collisions are also the reason for the high temperature of the plasma ranging from 6,000 to 10,000 K, depending on the region. The plasma comprises of positively charged argon ions and unbound electrons and can be considered neutral on the macroscopic scale, as it is only weakly ionized (~0.1 %) [12]. It is preserved as long as the radio frequency power is supplied to the copper coil. [12,13,25]

Due to the harsh temperatures of the ICP and the large amounts of energy transferred to the analytes, it is considered a hard ionization source and completely desolvates, vaporizes and atomizes most molecules in the sample. The degree of ionization, however, is contingent upon the temperature of the plasma, the electron number density and the ionization energy of the specific element relative to that of argon (15.76 eV). Higher temperatures and lower ionization potential yield higher degrees of ionization, as described by the Saha equation. Under hot plasma conditions, most of the elements in the periodic table are over 80 % ionized. As a consequence of their higher ionization potentials, a third of the elements are poorly ionized, e.g., “He, Ne, F, O and N (<1 %); Kr and Cl (1-10 %); C, Br, Xe and S (10-30 %) and P, I, Hg, As, Au and Pt (30-80 %)” [13]. While most elements produce singly charged ions, some elements such as Ce and Ba, have sufficiently low second ionization potentials to also generate doubly charged ions. [12,13,25]

Die approbierte gedruckte Originalversion dieser Diplomarbeit ist an der TU Wien Bibliothek verfügbar
The approved original version of this thesis is available in print at TU Wien Bibliothek.

2.2.3 Interface and Ion Optics

Mass separation requires a surrounding, where as few collision events as possible occur. Any collision can result in ions reacting (with the collision partner) or being neutralized, scattered or fragmented, all of which are undesirable under normal circumstances. It is for this reason that mass filters are usually operated at reduced pressures of 10^{-5}-10^{-9} mbar. On the other hand, ionization in the ICP is performed at atmospheric pressure. This necessitates the implementation of a sampling interface, which transports the analyte ions from the high-temperature, atmospheric pressure environment of the ICP to the room temperature, high-vacuum environment of the mass analyzer within a very short distance, in order to keep instruments compact. [12,13]

Figure 5 shows a schematic of such an interface. The ICP plasma hits the typically nickel-based, so-called sample cone, at the tip of which lies an aperture with a diameter of ~1 mm. An expansion chamber – connected to a rotary pump – is situated between the sample and the so-called skimmer cone. The reduced pressure (low mbar range) results in the plasma being drawn into the expansion chamber and to expand adiabatically, leading to the formation of a free jet. "The flow speed of the expanding gas exceeds the local speed of sound, resulting in supersonic expansion. The rapid increase in gas velocity requires energy, which is acquired by converting the thermal energy of the gas into kinetic energy […]" [12], meaning that the gas kinetic temperature drops to 100-200 K. Without going into further detail (cf. [12]), the also usually nickel-based skimmer cone with an aperture of 0.4-0.7 mm is placed <1 cm from the rear of the sample cone. [12]

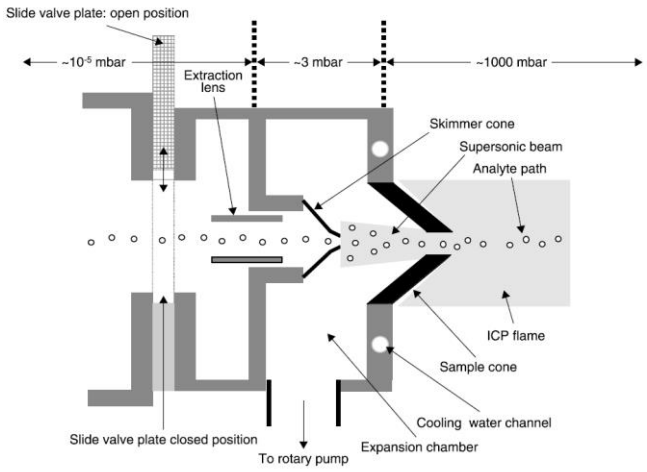

Figure 5: Sampling interface [12]. The positively charged, negatively charged or neutral species are sampled from ICP plasma by the sample cone. Adiabatic expansion occurs in the expansion chamber and the gas beam cools to 100-200 K. From there, the skimmer cone achieves the transition from a rough vacuum to the high-vacuum intermediate chamber.

Die approbierte gedruckte Originalversion dieser Diplomarbeit ist an der TU Wien Bibliothek verfügbar
The approved original version of this thesis is available in print at TU Wien Bibliothek.

The gas beam stemming from the ICP now enters a high-vacuum intermediate chamber, but still consists of positive ions, negative ions and neutral species. Either the positively or negatively charged ions can be analyzed further by employing electrical fields in a process termed extraction. However, positive ions are more beneficial for ICP-MS, as they are formed more efficiently for most elements of the periodic table. In order to extract the ions, a circular metal tube located close to the skimmer cone is set to a slightly positive or negative charge (+10 to -1000 V), accelerating the positive ions away from the gas beam towards the ion optics. At the same time, electrons are repelled and a beam of positively charged ions is formed. [12]

Within the intermediate chamber also lie the ion optics, which serve as a guide for the ions from the extraction lens towards the mass analyzer. The ion trajectories are dependent on both ion kinetic energy and space-charge effects, i.e., same-sign ions repel each other when in close proximity. Nevertheless, ion-focusing lenses are necessary, since scattered ions will ultimately not be detected. In principle, focusing is performed by applying constant electric fields between electrostatic lenses, shaped as metal discs with a central opening. This causes a gradient of equipotentials, which serve as refracting surfaces – in analogy to the optical counterparts. Alternatively, the ion can be focused by multipoles. The operating principle of a multipole is discussed in more detail for the quadrupole in the following chapter. [12,13]

All things considered, the transfer from the ICP to the MS is connected to an enormous loss of ions. Behind both sample and skimmer cone the sampled beam of ions expands such that the majority of the ions is discarded via the vacuum pumps. The ions that do pass the interface can then be extracted and shaped to a focused beam. Moreover, it has to be pointed out that low mass ions are affected more heavily by space-charge effects due to their lower kinetic energy. Hence, low mass ions “may be more readily ejected to the fringes of the beam or even lost all together”, reducing their sensitivity in particular. [12]

2.2.4 Mass Filter and Detection

Focused ion beams can be separated according to their mass-to-charge ratio by several different mass filters. In the context of ICP-MS, quadrupole, sector field and time-of-flight mass spectrometers are the most common, commercially available types. [12,23] As the mass analyzer of the instrument used for this thesis is a quadrupole, this type shall be elaborated on.

Die approbierte gedruckte Originalversion dieser Diplomarbeit ist an der TU Wien Bibliothek verfügbar
The approved original version of this thesis is available in print at TU Wien Bibliothek.
TU Bibliothek Your knowledge hub WIEN

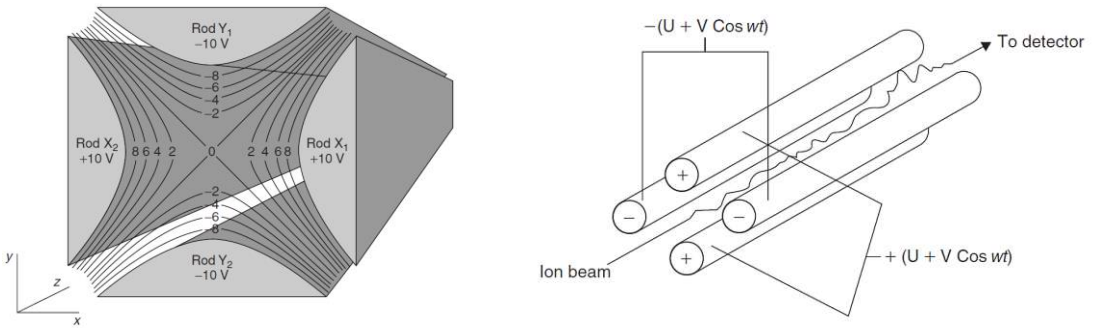

a) **b)**

Figure 6: a) Direct current field of a quadrupole mass filter [12]. The center of the circle spanned by the rods is effectively fieldless. b) Ion trajectory through the superimposed direct and alternating current field of the quadrupole mass filter [13]. According to the Mathieu equations, only specific values for the currents enable transmission of a particular ion.

In an idealized quadrupole mass filter, a potential of equal value but opposite polarity is applied to two pairs of electrodes as illustrated in Figure 6a). Disregarding fringing effects, that is, inconsistencies in field strength at entry and exit of the quadrupole, the potential only varies in the plane perpendicular to the rods, but not parallel. The potential distribution should preferably be generated by hyperbolic rods, but cylindrical rods suffice for most applications, despite setting up fields resulting from the linear superposition of the individual rods. Cylinders are preferred in practice as they are easier to manufacture and align. [12,13]

If the direct current field was to be applied to a stream of ions by itself, positive ions would be pulled to the negative rods and negative ions to the positive rods. Hence, for mass separation, the potential must consist of a constant and an alternating, time-dependent portion. This is shown in Figure 6b), where U is the direct current component and V is the applied radio-frequency current with its frequency ω. It is important to note that the alternating current of one pair of rods has the opposite phase compared to the other pair. At any point in time, ions are accelerated to one rod set, but when the radio-frequency field switches polarity, the ions are attracted to the other set of rods. If frequency and amplitude of the alternating current are chosen correctly, the ions will pass through the quadrupole. The underlying concepts were developed by Mathieu and the solution of the Mathieu equations allows for the definition of a stability region. This region corresponds to an interval of values for direct and alternating current, for which the trajectory of an ion with a specific mass and charge is stable, meaning that the ion is not lost and transmits through the mass filter. [12]

The trajectory of the ions is subject to field geometry, the amplitude and frequency of the alternating current, the magnitude of the direct current, the m/z value of the ions, the

Die approbierte gedruckte Originalversion dieser Diplomarbeit ist an der TU Wien Bibliothek verfügbar
The approved original version of this thesis is available in print at TU Wien Bibliothek.

velocity and distinct position of the ions as well as the phase angle. A major benefit of the quadrupole mass filter is the large angle of acceptance, i.e., ions within a 60 ° cone can enter into the mass analyzer. Furthermore, a quadrupole is compact and also not restricted to ions with a narrow kinetic energy distribution. It is however important to note that quadrupoles are sequential devices meaning that only one m/z ratio at a time can be analyzed. Finally, the mass-separated ions are registered by a detector. For this purpose Faraday cups as well as discrete-dynode/continuous-dynode electron multipliers are employed. The ICP-MS system used in this thesis contains a simultaneous mode discrete-dynode electron multiplier, which is discussed in the following. [13]

Essentially, electron multipliers are devices that convert ions into electrons in a process called secondary electron emission. Upon impact on a conversion dynode, an ion exiting the mass analyzer is converted into secondary electrons, which are then accelerated towards the next dynode of the multiplier, yielding more secondary electrons, and so on. This generates millions of electrons, which are captured by an output electrode in the shape of a pulse. The gain of an electron multiplier quantifies the signal enhancement and "can be defined as the average number of electrons collected at the multiplier's output electrode for each input ion that initiates an electron cascade". [12]

In simultaneous mode detection, the electron multiplier is divided into two sections. The first section operates in analog mode, amplifying the current with a gain of 10^4-10^6. A beam-splitting dynode diverts part of the electron cascade towards a Faraday cup, which consists of a collector electrode surrounded by a cage. The electron current is neutralized upon striking the electrode through a resistor and causes a potential drop, creating a signal. The remaining electron signal passes through the beam-splitting dynode to the pulse-counting mode section and is amplified further to a total gain of 10^6-10^8, before being collected at an output electrode and interpreted as a signal by ion-counting detection electronics. As the name suggests, analog and pulse-counting mode can be operated simultaneously, so that high ion count rates can be diverted to the Faraday cup, while low rates can be amplified further in the pulse-counting section. This is usually done automatically and improves the lifetime of the detectors. [12,13]

2.2.5 Formation and Reduction of Spectral Interferences in ICP-MS

ICP-MS is affected heavily by the formation of isobaric interferences of which two types exist. Firstly, elemental ions with the same nominal mass such as $^{87}Rb^+$ and $^{87}Sr^+$ overlap in

Die approbierte gedruckte Originalversion dieser Diplomarbeit ist an der TU Wien Bibliothek verfügbar
The approved original version of this thesis is available in print at TU Wien Bibliothek.

the mass spectrum. Secondly, elemental ions may overlap with polyatomic ions formed in the plasma. For instance, $^{40}Ar^{16}O^{+}$ interferes with $^{56}Fe^{+}$ (the most common stable isotope of iron) and $^{16}O_2^{+}$ with $^{32}S^{+}$ (the most common stable isotope of sulfur). The formation of these polyatomic ions is imminent considering that the ICP is in contact with the ambient atmosphere. For instance, carbon, nitrogen, oxygen and hydrogen from the ambient may collide with an analyte ionized by the ICP to produce the respective polyatomic ions. Moreover, doubly charged ions may also interfere singly charged ions, e.g., $^{46}Ti^{2+}$ for $^{23}Na^{+}$. This causes worse detection limits and may at worst hinder quantification for these isotopes. [12,19]

In order to reduce the impact of spectral interferences, mass spectrometers with high mass resolution, such as (double focusing) sector field and time-of-flight instruments, may be used. Quadrupole instrument offer poor mass resolution, but enable the implementation of so-called collision and reaction cells, which are situated in the intermediate chamber of the ICP-MS instrument. In principle, these cells consist of ion guides, e.g., hexapoles or octapoles, which are designed for high ion transmission and are pressurized with a specific gas. Within the cell, the ions are therefore faced with a neutral species, which:

- interacts/reacts with either the desired analyte or the isobaric interference so as to shift its mass (chemical resolution by reaction) or
- reduces the kinetic energy of the polyatomic ions by collision, i.e., kinetic energy discrimination (KED); as the collision cross-section of the polyatomic ions is larger, they lose more kinetic energy than monoatomic ions.

The two concepts are often intertwined, e.g., kinetic energy discrimination may aim to reduce the interferences produced by reactions within the cell. “Since the product ions that have exited the cell have lower kinetic energy than the atomic analyte ions under non-thermal conditions, they are selectively blocked by [a] potential barrier of appropriate height after the cell.” [26] The energy barrier is usually established by setting the direct current bias voltage of the subsequent quadrupole analyzer more positive than the ion guide of the cell. What is more, the ion kinetic energy spread is narrowed through the collisions, which improves sensitivity in the mass analyzer. [12,26,27]

The choice of gas in the collision/reaction cell is not trivial. In general, the gas should have a low atomic/molecular mass in order to reduce collisional scattering along the transmission axis to the mass analyzer. Simply applying a collision gas can enhance the sensitivity by a factor of 5 to 10 as interferences generated in the plasma or at the interface are suppressed. When aiming to suppress a specific interference, reaction gases such as H_2,

Die approbierte gedruckte Originalversion dieser Diplomarbeit ist an der TU Wien Bibliothek verfügbar
The approved original version of this thesis is available in print at TU Wien Bibliothek.
TU Bibliothek Your knowledge hub WIEN

CH_4 or NH_3 are common, while He is customary for simple KED purposes. With this technology, quadrupole-based ICP-MS systems have a significant advantage compared to high resolution ICP-MS (HR-ICP-MS), which employs its magnetic field to tackle isobaric interferences. The pair of $^{87}Rb^+$ and $^{87}Sr^+$ cannot be resolved by HR-ICP-MS, but by CH_3F gas in a reaction cell positioned ahead of a quadrupole-based ICP-MS, because Sr^+ is shifted to SrF^+. [12,13,26,27]

2.2.6 Using Polyatomic Species as an Advantage

In sharp contrast, this thesis is concerned specifically with the utilization of these usually unwanted isobaric interferences, or, to be more precise, polyatomic ions. An example for the use of polyatomic ions are the works of Jamari et al. [28-30]. In this case, the effluent of a high-pressure liquid chromatography column containing fluoride-based samples was mixed online with barium solutions in order to produce the polyatomic ion $^{138}Ba^{19}F^+$ within the ICP plasma. Since fluorine has a higher ionization potential than argon, little $^{19}F^+$ is produced in a positive ion mode argon plasma. Besides, interferences such as "$^1H_3{}^{16}O^+$, $^1H^{18}O^+$ and $^1H_2{}^{17}O^+$" increase the background at m/z 19 [28]. This issue can be mitigated by using negative ion mode apparatus, but most commercial instruments only allow for positive ion mode operation. With the method proposed by Jamari et al. an LOD in the low $\mu g \cdot L^{-1}$ corresponding to the low ng range was obtained, which is a significant improvement on both negative ion mode and high resolution ICP-MS. [28]

As mentioned in the introduction, the aim of this thesis is to employ the molecular ion $^{40}Ar^2D^+$ to determine the deuterium content of solids. This concept was developed and has already been applied for mixtures of deuterium-depleted water and deuterium-enriched water by Galbács et al. [15]. In their work, the equilibrium concentrations of different atomic hydrogen, deuterium, argon and oxygen species as well as molecular species of the aforementioned elements within the plasma were modelled. "The model clearly predicted that species at mass 4 (D_2^+ and H_2D^+) and mass 42 (ArD^+) have the greatest potential for use in quantitative analytical measurements […]" [15]. In their experiments, m/z 42, that is, the molecular ion $^{40}Ar^2D^+$, delivered high signal intensities, which even allowed for the quantification of deuterium in the samples.

Die approbierte gedruckte Originalversion dieser Diplomarbeit ist an der TU Wien Bibliothek verfügbar
The approved original version of this thesis is available in print at TU Wien Bibliothek.

3. Experimental

3.1 Laser Systems

Two different Nd:YAG lasers were used for ablation throughout the experiments, since it was unclear which system would actually perform better for this topic. First, a NWR213 laser system (Elemental Scientific Lasers, CA, USA; see Figure 7a)) with the frequency quintupled wavelength of 213 nm and a pulse duration of 4 ns was used, connected by PTFE tubing to the ICP-MS. Ablation was performed under helium, whilst also employing argon as make-up gas right before feeding the ablated material into the ICP-MS. Fast washout is achieved by a so-called ablation cup positioned above the sample.

Secondly, a LIBS J200 system (Applied Spectra, Inc., CA, USA; see Figure 7b)) with a wavelength of 266 nm and a pulse duration of 6 ns was utilized. The key word LIBS is a hint that the J200 is primarily used for LIBS studies, but it can also be employed solely for laser ablation as well as simultaneous LA-ICP-MS and LIBS (a technique coined Tandem LA-ICP-MS/LIBS). Helium and argon could be chosen as gas in the ablation chamber; a nebulizer-like contraption sitting close to the chamber enabled addition of either helium as ablation gas and argon as make-up gas or vice versa. The former was deemed more feasible, because the argon-based ICP-MS only allows for low amounts of helium to be introduced and the main purpose of the make-up gas – in this case – was the *faster* transport of ablated material to the ICP-MS. The tubing connecting to the ICP-MS was again PTFE-based. It should be mentioned here, that the total gas flow to the ICP-MS can change the position of the ICP plasma and therefore influence signal intensity.

a) **b)**

Figure 7: a) NWR213 [31] and b) LIBS J200 laser system [32] used for laser ablation.

Die approbierte gedruckte Originalversion dieser Diplomarbeit ist an der TU Wien Bibliothek verfügbar
The approved original version of this thesis is available in print at TU Wien Bibliothek.

Both apparatus contained a movable stage allowing for accurate control of ablation patterns in all three spatial dimensions, whilst using microscope camera optics enabled the positioning and tracking of ablation patterns. The parameters for these patterns were set via the system software Active View™ by New Wave Research, Inc. (NWR213) and Axiom 2.0 by Applied Spectra, Inc. (LIBS J200), respectively. The respective lasers both produced circular beams.

3.2 Ablation Cell

The laser systems both contain an ablation chamber that enables the transport of ablated material to the ICP-MS. In the case of the NWR213 system, this ablation chamber allows for the introduction of multiple samples and the ablation ejecta are drawn away from the sample by the ablation cup, which facilitates suitable wash-out for most applications. However, organic species that are released by tubing, sealings etc. result in large backgrounds for elements like carbon. In terms of the LIBS J200, the large volume of its ablation chamber can accommodate a large number of samples, but is significantly compromised in terms of wash-out efficiency. Preliminary experiments with the LIBS J200 system lead to the conclusion that leakage from the ablation chamber is possible, bringing about decreased signal intensities – at times even no intensity above noise at all. All things considered, a different confinement for the ablation process had to be found.

This issue was resolved by using an *ablation cell* produced in-house by Johannes Frank, illustrated in Figure 8. An aluminum block was shaped in such a way that a sample could be placed in its cavity with a diameter of 11 mm and a depth of 5 mm. Therefore, the ablation volume of the ablation cell was 0.475 cm^3. Atop the cavity, gas tightness of the cell was ensured by virtue of a fused silica window being screwed tightly to a rubber sealing ring (fitting in a groove) by the aluminum cell cover with four Allen screws. Furthermore, for the transport of ablated sample to the ICP-MS, two opposing openings were equipped with Festo QSM-M5-4 push-in fittings connecting to the PTFE tubing. The flow of incoming ablation gas was regulated via the mass flow controller within the LIBS J200 system, making the use of helium as well as argon possible. The ablation cell fit in both laser systems.

3.3 Cryostage

The study of water uptake by polymers required the samples to be cooled so as to minimize desorption of water while they were placed in the sample cavity and flushed with dry carrier

Die approbierte gedruckte Originalversion dieser Diplomarbeit ist an der TU Wien Bibliothek verfügbar
The approved original version of this thesis is available in print at TU Wien Bibliothek.

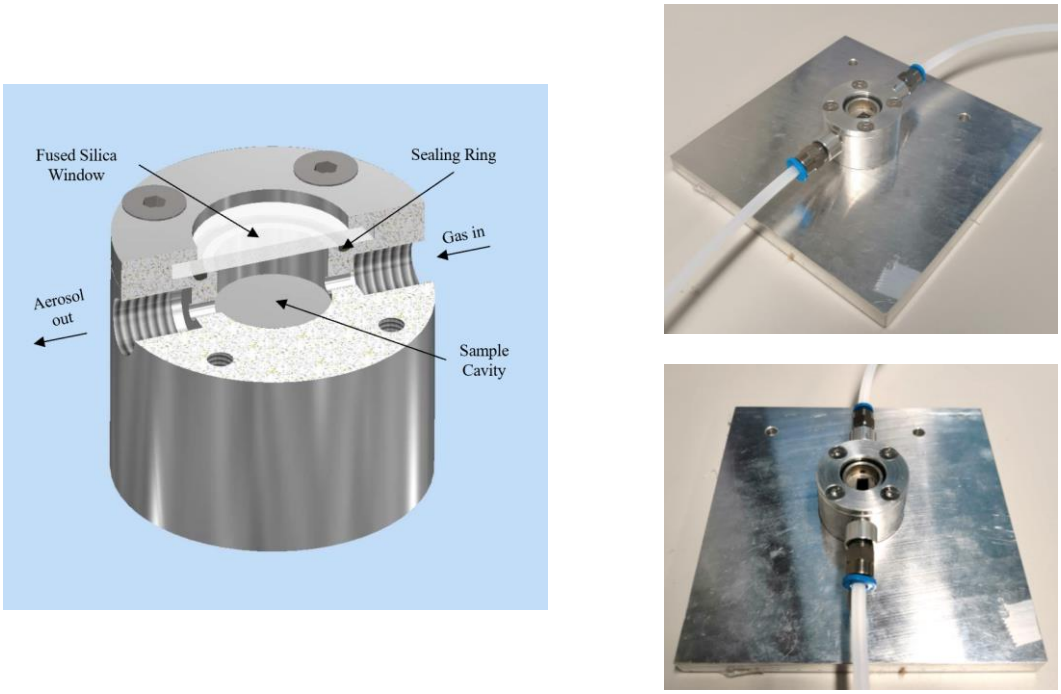

a) **b)**

*Figure 8: Cell design for ablation experiments in the **ablation cell**; a) concept drawings, b) real-life pictures with tubing connected. The sample is placed in the sample cavity and irradiated by the laser through the fused silica window. A stream of carrier/ablation gas, introduced via the gas inlet, ensures transport of the produced sample aerosol to the ICP-MS.*

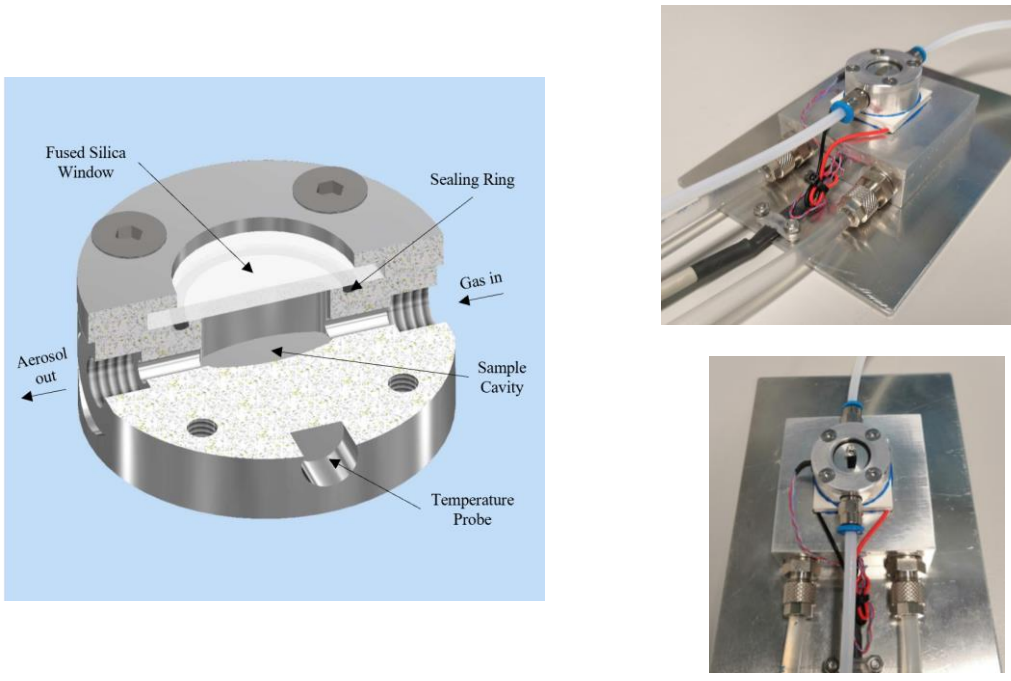

a) **b)**

*Figure 9: Cell design for ablation experiments in the **Cryostage**; a) concept drawings, b) real-life pictures with tubing connected. The ablation cell used here has an oval sample cavity to improve wash-out.*

Die approbierte gedruckte Originalversion dieser Diplomarbeit ist an der TU Wien Bibliothek verfügbar
The approved original version of this thesis is available in print at TU Wien Bibliothek.

gas (cf. 4.3 for a detailed discussion). For this purpose, a different dell design was used, which was also fabricated in-house by Johannes Frank and is illustrated in Figure 9. The oval sample cavity design aims to improve wash-out properties further, possibly allowing for imaging applications. In collaboration with Wolfgang Tomischko, this cell was attached to a Peltier cooling element (ETH-127-10-13-S-HI by Adaptive®, United Kingdom), which in turn was joined to an aluminum-based heat exchanger. The heat exchanger was operated with room temperature water and served as a heat-sink for the hot side of the Peltier element, facilitating long-term temperature stability of the cell. An external monitoring device enabled temperature adjustment, while the actual temperature was determined by a probe sitting in the cell casing (see Figure 9b)). The overall construction is termed C*ryostage* in the following. With the Cryostage, temperature stability at -10 °C was guaranteed for several hours. Like with the ablation cell, the Cryostage could be used in both laser systems.

3.4 ICP-MS-System

ICP-MS data was gathered by a Thermo iCAP™ Qc instrument (ThermoFisher Scientific, Germany; see Figure 10) in selected-ion monitoring mode. The iCAP Qc uses a quadrupole as mass analyzer, whilst also containing a flatapole-based collision/reaction cell enabling kinetic energy discrimination (cf. 2.2.5). In unpressurized operation, that is, without reaction or collision gas, the flatapoles act as ion guides. Data acquisition was performed with Qtegra™ by Thermo Fisher Scientific. For solid sampling the LA systems or ablation cells were connected to the instrument via PTFE tubing. Instrument parameters were optimized regularly for maximum ^{115}In signal measuring a piece of NIST® Standard Reference Material® 612 (National Institute of Standards and Technology, USA). Dry plasma conditions were maintained for all measurements. The general ICP-MS operating parameters are given in Table 1.

Table 1: ICP-MS operating parameters for the measurements. † marks isotopes that were measured to rule out contribution of calcium to the $^{40}Ar^2D^+$ signal. †† marks the isotopes measured for film standards in an effort to use platinum as an internal standard.

Parameter	Value
RF power	1550 W
Auxiliary gas flow	0.8 L·min^{-1}
Cool gas flow	14 L·min^{-1}
Measured Isotopes	^{13}C, ^{42}Ca (=$^{40}Ar^2D^+$), ^{43}Ca†, ^{48}Ca†, ^{196}Pt††, ^{198}Pt††
Dwell time for each mass	10 ms (50 ms for ^{42}Ca)

Die approbierte gedruckte Originalversion dieser Diplomarbeit ist an der TU Wien Bibliothek verfügbar
The approved original version of this thesis is available in print at TU Wien Bibliothek.

Figure 10: iCAP™ Q instrument with equipment for sample introduction by solution nebulization [33].

3.5 Standard Preparation

Pellets and polymer-based thin films were prepared for method development in order to optimize the laser ablation and ICP-MS parameters. Afterwards, new sets of standards were produced so as to perform calibration. The following chemicals were used:

- Polyimide P84 (HP Polymer GmbH); hereinafter: polyimide
- Poly(methyl methacrylate) (Acros Organics, avg. M.W. 35,000); hereinafter: PMMA
- N-Methyl-2-pyrrolidone (Merck, p.a.); hereinafter: NMP
- Benzoic acid (Fluka, 99 %)
- Benzoic acid-2,3,4,5,6-d_5 (Sigma-Aldrich, ≥99 atom% D); hereinafter: deuterated benzoic acid
- Platinum(II) bis(acetylacetonate) (Acros Organics, 98 %); hereinafter: Pt-acac
- Silicon wafers (Infineon Austria AG, cut into 10 × 10 mm pieces, high purity, n-doped).

Ablation parameters such as laser energy, ablation gas flow, the specific experiment setup etc. are noted in the results section.

3.5.1 Pellets

Initial experiments with pellets, prepared by mixing polyimide and deuterated benzoic acid in arbitrary amounts, made clear that the ablation characteristics differed drastically from pellet to pellet. As a consequence, pellets were produced, in which the amount of polyimide was held constant and the rest was made up of a mixture of arbitrary amounts of deuterated and non-deuterated benzoic acid. Similarly to the initial pellets, the mixture of solids was ground by a Retsch MM 400 oscillating ball mill (Retsch GmbH, Germany) in a grinding cylinder with balls as grinding medium, both of which were tungsten carbide based. The samples were ground at 20 Hz for 2 min and then pressed uniaxially with a pressure of

Die approbierte gedruckte Originalversion dieser Diplomarbeit ist an der TU Wien Bibliothek verfügbar
The approved original version of this thesis is available in print at TU Wien Bibliothek.

200 bar. In order to fit into the ablation cell, the pressed pellets had to then be broken into four pieces.

3.5.2 Polymer Films

Since the pellets were rather unlike the desired application sample in terms of shape and ablation behavior, the attention was shifted towards polymer-based thin films. Pt-acac was dissolved in NMP and further diluted with NMP to the desired concentration in an effort to introduce platinum as internal standard. Benzoic acid and deuterated benzoic acid were then dissolved in the diluted Pt-acac solution. PMMA and polyimide were dissolved in NMP and then mixed with the (deuterated) benzoic acid solutions in equal amounts to give a nominal weight of 200 mg. As with the pellets, the amount of polymer was held constant; hence, a possible standard solution contained 100 mg of PMMA or polyimide as well as 50 mg of benzoic acid and 50 mg of deuterated benzoic acid solution. All solutions were thoroughly homogenized by using a vortex and an ultrasonic bath.

To fit into the ablation cell, the 1 × 1 cm Si wafers were broken up into approx. 5 × 5 mm squares for the experiment with the ablation cell. For experiments with the Cryostage, the wafers had to be broken into rectangles in sizes of approx. 5 × 3 mm. 5 µL or 7.5 µL of the standard solution were pipetted onto the wafer pieces for experiments with the Cryostage or ablation cell, respectively. The polyimide standards were dried at 100 °C for 30 min on a heating plate to evaporate the NMP, before slowly being cooled to room temperature by simply turning off the heating; the PMMA standards were dried at 100 °C for 1 h.

3.6 Water Absorption Samples

In order to test for water absorption, polyimide samples had to be subjected to D_2O and analyzed in the Cryostage. Three different types of polyimides were provided by an industrial partner and are denoted PI 1, PI 2 and PI 3 in the following. The polyimides formed a film with 11 µm thickness atop 1 × 1 cm Si wafers; hence, the wafers had to be broken into approx. 5 × 3 mm pieces to fit into the Cryostage.

Initially, some pieces were submerged in no less than 1 g deuterium oxide for at least 96 h. After removing the samples from the heavy water, excess liquid was wiped off from the surface and the samples were then frozen to -18 °C, all within 2 min. After 24 h in the freezer, the samples were placed into the argon-flushed Cryostage, which was operated at a maximum of -12 °C, within 2 min before analyzing the samples.

Die approbierte gedruckte Originalversion dieser Diplomarbeit ist an der TU Wien Bibliothek verfügbar
The approved original version of this thesis is available in print at TU Wien Bibliothek.
TU Bibliothek Your knowledge hub WIEN

4. Results and Discussion

This section aims to provide an overview of the results of this thesis, whilst additionally serving as a chronology. In the beginning of the practical work, the aim was to produce standards with significant deuterium content so as to determine whether analyzing deuterium via the polyatomic $^{40}Ar^{2}D^{+}$ ion is actually possible.

In fact, electrothermal vaporization (ETV) was initially used as sample introduction system for the ICP-MS. The hypothesis was that, if polymers were submerged in D_2O, the absorbed heavy water could be evaporated in a controlled manner by using a short temperature ramp in the ETV instrument. However, since the D_2O condensed in the transfer lines and did not wash out of the system in a reasonable amount of time, the background at m/z 42 was so large that the signal from the temperature program was often insignificant.

The focus was then shifted towards trying to freeze the deuterium oxide in the polymer by using a predecessor of the Cryostage (cf. 3.3), which could be inserted into the NWR213 laser. Despite cooling the polymers to -5 °C, the main disadvantage of this cooling stage was the low temperature stability, which resulted in a quick temperature increase within minutes. Once again, the large background at mass 42 prevented proper evaluation.

Subsequently, it was decided to introduce deuterium in solid form. For this purpose, pellets consisting of a mixture of potassium dideuterium phosphate (KD_2PO_4) and cellulose were produced and measured by LA-ICP-MS, but the results were unusable. Further experiments, such as swelling gelatin and hydrating anhydrous copper sulfate with D_2O were also unsuccessful. The latter was a promising approach since LIBS measurements revealed a clearly visible deuterium band, but the background at mass 42 – most probably resulting from D_2O evaporation – hindered ICP-MS analysis once more.

The acquisition of deuterated benzoic acid proved to be a vital step towards quantifying deuterium in the desired standards. Initial experiments, in which the deuterated benzoic acid was mixed in arbitrary amounts with the commercial PI powder clearly showed a significant signal at mass 42 above a comparatively small background. This standard preparation method was then refined, before addressing the fabrication of film standards as set out in the experimental section (cf. 3.5). In the following, measurements of these standards, including calibration curves allowing for the quantification of deuterium, are shown, ablation atmospheres compared and internal standardization discussed. Afterwards, the distinct types

Die approbierte gedruckte Originalversion dieser Diplomarbeit ist an der TU Wien Bibliothek verfügbar
The approved original version of this thesis is available in print at TU Wien Bibliothek.

of bonding of deuterium in standards and sample are explained as well as how this impacts sample analysis, before providing the results of water absorption experiments.

4.1 Quantification in Pellets

In an attempt to achieve high signal intensity for m/z 42, both laser systems were employed to ablate the pellet standards in the ablation cell. Different ablation parameters were tested by performing line scans across the pellet surface. However, it quickly became clear that elevating the ablation rate by increasing the laser energy/fluence, for instance, did not necessarily correspond to higher signal intensities. The main reason behind this was a noticeable rise in particle settlement by virtue of redeposition of ablated material around the ablation crater and further on in the ablation cell. As a consequence, a yellow hue originating from the polyimide matrix appeared both in the ablation cell and the transport lines. It was decided to compromise signal intensity for better transport efficiency as the material at times clogged the transfer line. A trivial solution would be to increase the argon gas flow, but confusingly, this did not improve transport efficiency. Conceivably, this may be due to an inadequate flow regime in the ablation cell for the transport of the particles generated during these experiments ([34]), which leads to large wash-out times from the ablation cell. The parameters ultimately used to analyze the pellet standards are given in Table 2.

4.1.1 Discussing General Features of the Generated Signal

As set out in 3.5.1, pellet standards were produced by combining polyimide powder with different mixtures of regular and deuterated benzoic acid. Several iterations of the preparation procedure were undertaken, but in the following only the results of the last series of standards are given. For this particular experiment, six standards with an approximate polyimide content of 800 $mg \cdot g^{-1}$ and a total weight of ~260 g were produced. The remaining mass was made up of six different mixtures of deuterated and regular benzoic acid, whereby the concentration of deuterated benzoic acid covers a region of 0-200 $mg \cdot g^{-1}$, corresponding

Table 2: Parameters used for the ablation of pellet standards. Ablation was carried out in the ablation cell.

Parameter	NWR213	LIBS J200
Laser fluence ($J \cdot cm^{-2}$)	2.2	8.9
Spotsize (µm)	150	100
Repetition rate (Hz)	20	10
Scan-speed ($mm \cdot s^{-1}$)	0.1	0.2
Ablation atmosphere	0.2 $L \cdot min^{-1}$ argon	

Die approbierte gedruckte Originalversion dieser Diplomarbeit ist an der TU Wien Bibliothek verfügbar
The approved original version of this thesis is available in print at TU Wien Bibliothek.

to a deuterium concentration of 0-16 $mg \cdot g^{-1}$. The standards were then ablated in the ablation cell with six individual line patterns with the purpose of achieving a somewhat transient signal, considering that only bulk information was of interest at this point.

In Figure 11 the ICP-MS signal intensities of ^{13}C and the mass corresponding to $^{40}Ar^{2}D^{+}$ are depicted, which represent three ablation lines of a standard containing 0 $mg \cdot g^{-1}$ and 16 $mg \cdot g^{-1}$ added deuterium, respectively. Additionally, these graphs act as comparison between the NWR213 and LIBS J200 laser. The carbon signal indicates that transport of the ablated material to the ICP-MS is achieved for all measurements. When comparing the ^{13}C signal of the left columns of Figure 11a) and b), it becomes clear that the higher energy output of the LIBS J200 laser causes higher ablation rates. However, a higher intensity at the mass corresponding to the $^{40}Ar^{2}D^{+}$ ion can also be observed. This is somewhat surprising as this specific standard should nominally contain no deuterium. Despite that sentiment, both polyimide and regular benzoic acid are expected to contain the natural abundance of deuterium, which amounts to approx. 0.15 $mg \cdot g^{-1}$ of the hydrogen bound in the respective substance (cf. [14] and 1.). Hence, it is not surprising that a background appears during each ablation pattern, but it remains unclear if naturally abundant deuterium is the only input.

With regards to the differences between the two standards shown in Figure 11, it is clear to see for both lasers that the signal intensity at mass 42 is larger for the standard with the higher deuterium concentration. Considering that this signal increase is more than one order of magnitude for the LIBS J200 laser – cf. the left and right column of Figure 11b) –, the only feasible explanation is the formation of the $^{40}Ar^{2}D^{+}$ ion. This is further backed up by Figure 12, where the signal intensities at m/z 42, 43 and 48 of the same two standards (0 and 16 $mg \cdot g^{-1}$ added deuterium) are illustrated. The natural abundance ratio of calcium isotopes on earth is 0.647 % for ^{42}Ca, 0.135 % for ^{43}Ca, and 0.187 % for ^{48}Ca [35,36]. Despite the abundances of ^{43}Ca and ^{48}Ca being lower than that of ^{42}Ca by a factor of 4.8 and 3.5, respectively, signal intensity above the background should be detected for all isotopes, if calcium is in fact present in the sample. However, this is by far not the case; the signal intensities for ^{43}Ca and ^{48}Ca most likely resemble the general background for these specific ICP-MS parameters.

The discussion shall now focus on the general shape of the $^{40}Ar^{2}D^{+}$ signal itself. Ideally, sample introduction via laser ablation results in ICP-MS signals that resemble box functions for lines ablated on a homogeneous sample. However, this is generally not the case

Die approbierte gedruckte Originalversion dieser Diplomarbeit ist an der TU Wien Bibliothek verfügbar
The approved original version of this thesis is available in print at TU Wien Bibliothek.

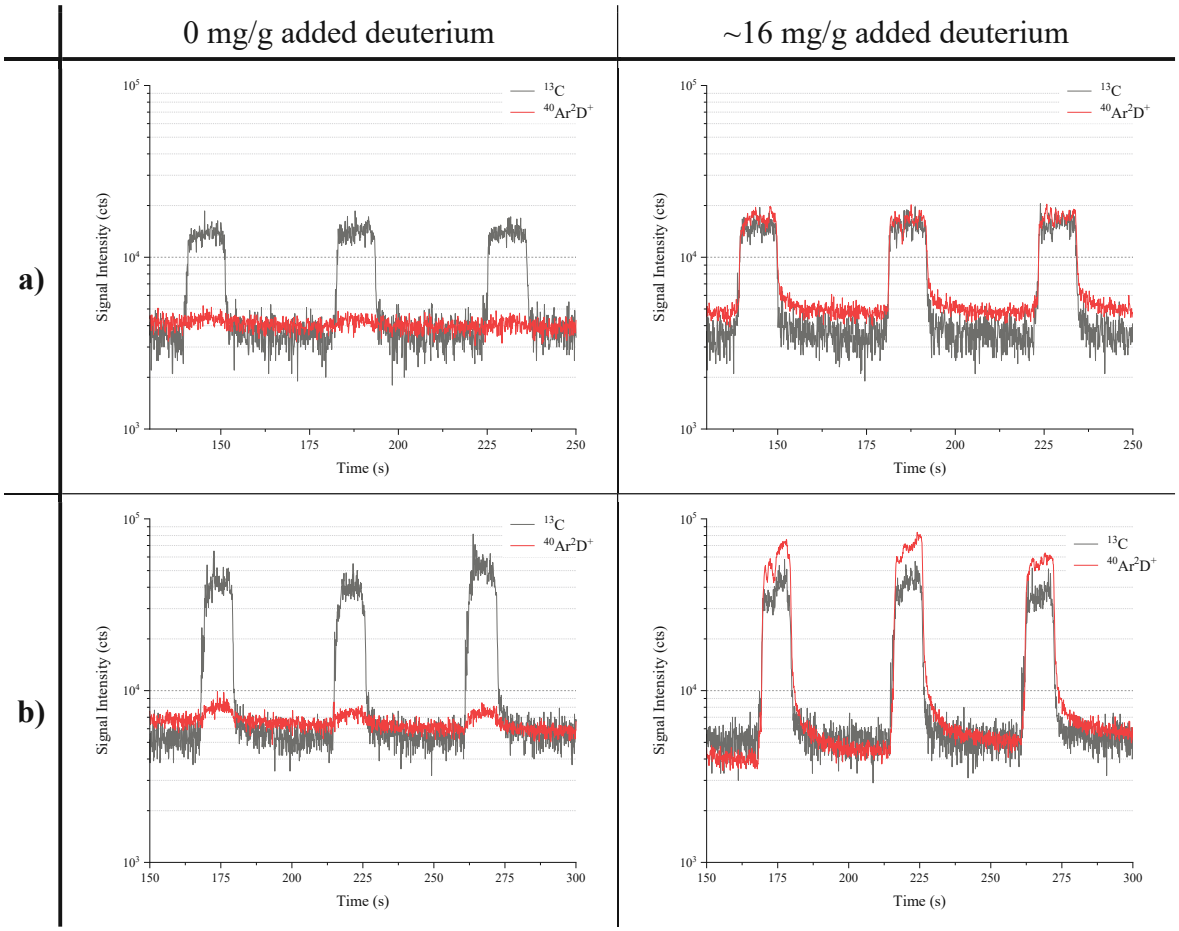

Figure 11: Signal intensities of ^{13}C (black) and $^{40}Ar^2D^+$ (red) for pellet standards containing no added deuterated benzoic acid (left column) and approx. 9 mg·g^{-1} added deuterium (right column), ablated with a) the NWR213 and b) the LIBS J200 laser. For both standards, the signal intensities resulting from three separate line patterns are shown. Ablation was carried out in the ablation cell.

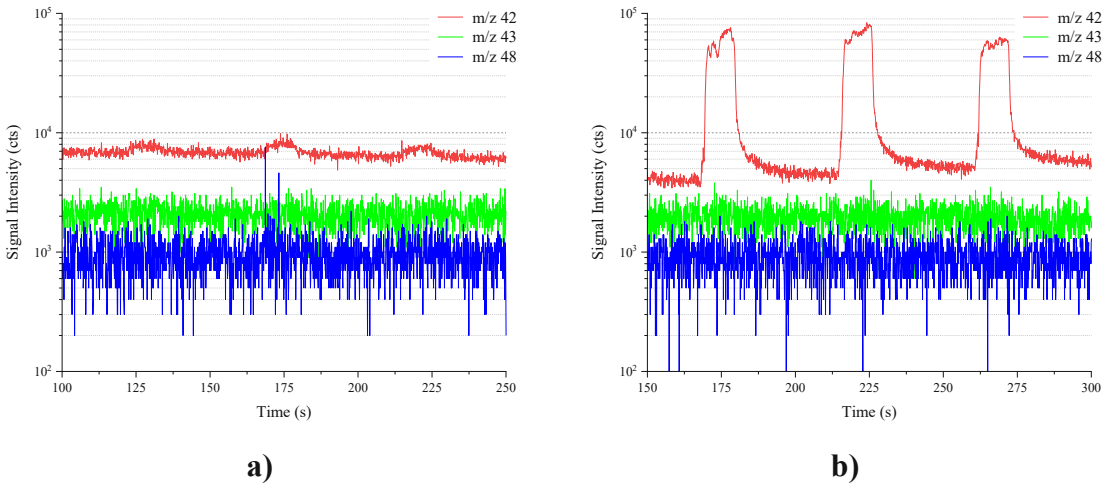

Figure 12: Comparison of the signal intensities at mass 42 (red), 43 (green) and 48 (blue) for pellet standards. For this figure the signal intensities of the pellet standards with a) 0 and b) 16 mg·g^{-1} added deuterium were plotted.

Die approbierte gedruckte Originalversion dieser Diplomarbeit ist an der TU Wien Bibliothek verfügbar
The approved original version of this thesis is available in print at TU Wien Bibliothek.

since wash-out effects occur. The initial diameter of a cloud of ablated material is determined by both laser energy and the pressure of the atmosphere surrounding the ablation site. This diameter determines the temporal width of the ICP signal, which lies in the low ms range. In contrast, when the sample aerosol is directly injected into the ICP-MS, "the temporal response of the [ICP-MS] system is limited by the wash-out time of the [ablation] cell, which normally exceeds several seconds." [34] The broadening of the signal is a direct result of mixing in the ablation chamber. For turbulent flow, particles can be distributed across the entire ablation volume such that the particles are introduced into the ICP in small portions, i.e., not every particle generated during the laser ablation process will arrive simultaneously at the ICP-MS. [34]

Note that the amount of material ablated by line scans across the surface of a pellet is comparatively large. The produced pellets can readily be broken apart as a consequence of their low mechanical stability, meaning that the impingent laser beam can liberate large particles in large quantities. This may also be a reason why the plateaus of the ablation patterns in Figure 11b) are not straight lines: the formed ablation crater is very irregular compared to polymer films, for example, because particle agglomerates beyond the ablation crater are randomly released from the surface too (cf. 4.2). If these agglomerates are transported to the ICP, this leads to a boost in signal intensity and henceforth an unstable signal. Furthermore, the substantial amount of ejecta gives rise to large wash-out times, best seen in Figure 11b) for the standard with high deuterium concentration. These wash-out times are far from the state of art for LA-ICP-MS. However, it is important to highlight that they are still significantly lower than experienced by Galbács et al. ([15]) by orders of magnitude. Despite analyzing samples with approximately the same deuterium content, laser ablation utilizes larger carrier gas flow rates (hundreds of $mL \cdot min^{-1}$) compared to the peristaltic pump flow rates ($\mu L \cdot min^{-1}$) employed for solution nebulization of liquid samples. Hence, the suboptimal wash-out of the samples from the ablation cell is still an improvement on liquid ICP-MS.

4.1.2 Calibration

Despite the issues raised in the previous chapter, the pellet standards allowed for the creation of a calibration curve. For this purpose, the signal intensities of both $^{40}Ar^{2}D^{+}$ and ^{13}C were analyzed. The parameters used resulted in an ablation pattern that lasted for 10 s. Of the generated ICP-MS signal, 5 s in the middle were averaged to arrive at a signal intensity for a single line pattern, whilst correcting for the blank signal without ablation by utilizing a 5 s

Die approbierte gedruckte Originalversion dieser Diplomarbeit ist an der TU Wien Bibliothek verfügbar
The approved original version of this thesis is available in print at TU Wien Bibliothek.
TU Bibliothek Your knowledge hub WIEN

region ahead of every individual ablation pattern. In total, six lines were ablated on every standard and then averaged to obtain respective linear regressions for both laser systems.

In Figure 13 the calibration curves based on average $^{40}Ar^{2}D^{+}$ signal intensity are illustrated. As a result of the lower laser fluence of the NWR213 laser, less material is ablated and lower signal intensity is obtained, which also impacts sensitivity as seen for the black line. This may also contribute to the supposedly superb linear fit for the NWR213. Even when reducing the scale of the ordinate, only small standard errors are observed. In contrast, the data for the LIBS J200 reveals larger standard errors, especially for standards with higher concentration. It has to be mentioned that the LIBS J200 laser at times suffers with inconsistent power output, i.e., the energy of the laser can differ quite drastically between patterns ablated with the same nominal ablation parameters. Hence, the amount of ablated material varies from pattern to pattern and different signal intensities are obtained in the ICP-MS. In an effort to reduce the signal variations, the $^{40}Ar^{2}D^{+}$ signal was normalized to that of ^{13}C. Essentially, carbon is used as an internal standard to correct for differences in ablation rate, an approach that has been discussed heavily in literature [37-39]. Makino and Nakazato provide the following reasons why the use of carbon as internal standard may not be suitable for polymer samples [39]:

- contrary to trace elements, carbon is partially transported as a gas and
- "carbon has high ionization energy (11.3 V) and is susceptible to matrix effect [*sic*]".

Deiting et al. found that carbon can correct for some effects caused by ablation, e.g., the interaction of the laser with the sample, but not for differences in the absorption properties of the sample that occur due to additives. However, Makino and Nakazato point out that internal standardization to carbon can be performed reliably for a variety of polymers when applying high laser fluences (>8 $J \cdot cm^{-2}$) [39].

Calibrations based on the normalized signal intensity are depicted in Figure 14. In this case, the $^{40}Ar^{2}D^{+}/^{13}C$ signal intensity ratio (determined by Qtegra^{TM}), was averaged across the same 5 s part of the ablation pattern as the average intensity in Figure 13. Unsurprisingly, normalization moves the two curves closer together since the carbon signal was lessened too for the NWR213 laser. Advantageously however, the signal differences between individual LIBS J200 ablation patterns and as a consequence the standard error for the standards was decreased. Hence, it can be concluded that normalization improves precision for measurements of the pellet standards.

Die approbierte gedruckte Originalversion dieser Diplomarbeit ist an der TU Wien Bibliothek verfügbar
The approved original version of this thesis is available in print at TU Wien Bibliothek.

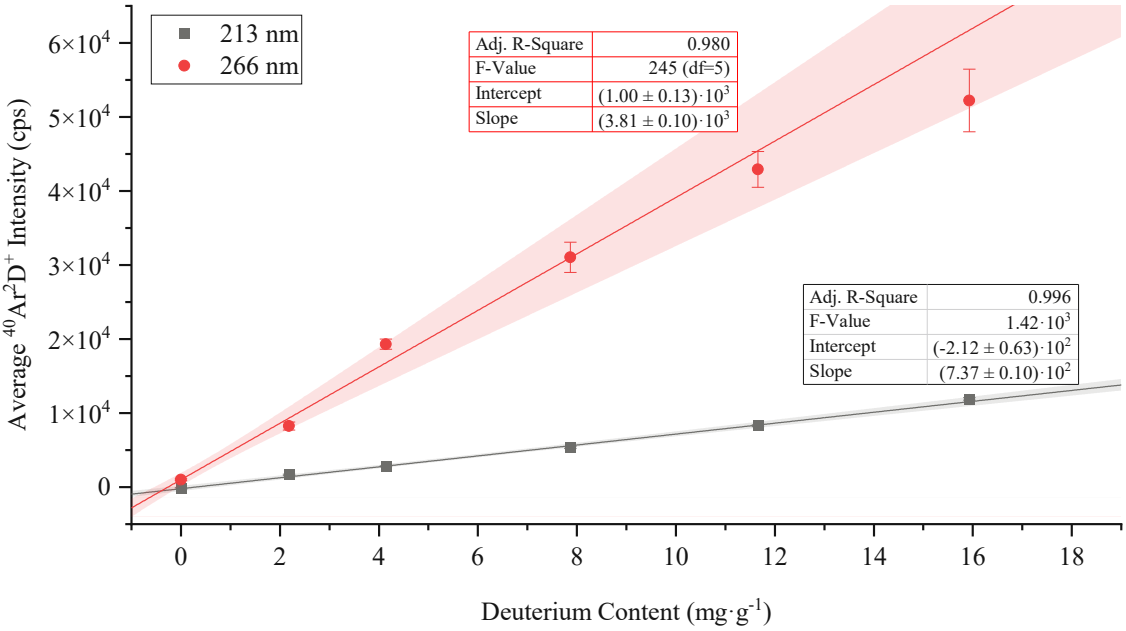

Figure 13: Pellet standard calibration based on average intensity of the $^{40}Ar^2D^+$ signal for the NWR213 (black) and LIBS J200 laser (red). The error bars represent the standard error of six individual measurements. Ablation was carried out in the ablation cell.

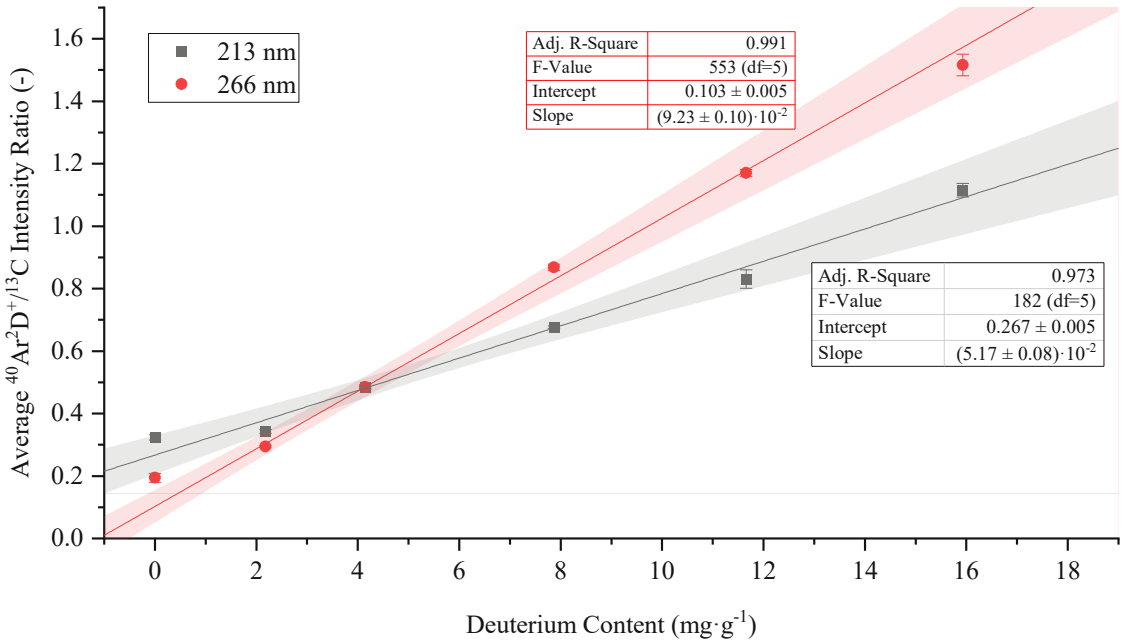

Figure 14: Pellet standard calibration based on the average $^{40}Ar^2D^+/^{13}C$ intensity ratio (corresponding to the normalized $^{40}Ar^2D^+$ signal) for the NWR213 (black) and LIBS J200 laser (red). The error bars represent the standard error of six individual measurements. Ablation was carried out in the ablation cell.

Die approbierte gedruckte Originalversion dieser Diplomarbeit ist an der TU Wien Bibliothek verfügbar
The approved original version of this thesis is available in print at TU Wien Bibliothek.

4.2 Quantification in Polymer Films

Despite manifesting that analyzing and quantifying deuterium in solids is possible, the main issue with pellet standards is their vastly different ablation behavior compared to polymer films. For instance, chapter 2.1.1 included a brief discussion on how different particle generation mechanisms can occur during laser ablation. A comparison between line scans on the surface of a pellet and film standard is shown in Figure 15 and there seems to be a dissimilarity between the two substrates. For the film standard, the main particle generation mechanism seems to be sample vaporization and recondensation. In the case of the pellet, a considerable amount of particles, that are loosely attached to the compacted surface, seem to break away as a consequence of the laser's shockwave, which is indicated by the fuzzy border of the ablation craters. LA-ICP-MS is highly dependent on matrix effects during laser ablation and ionization of the sample aerosol, impelling the analysis of matrix-matched standards, i.e., standards, whose matrix mimics that of the investigated sample – "otherwise, reliable quantification cannot be guaranteed" [23]. Ideally, certified reference materials would be utilized, but for this topic – like in many cases – no such reference material exists.

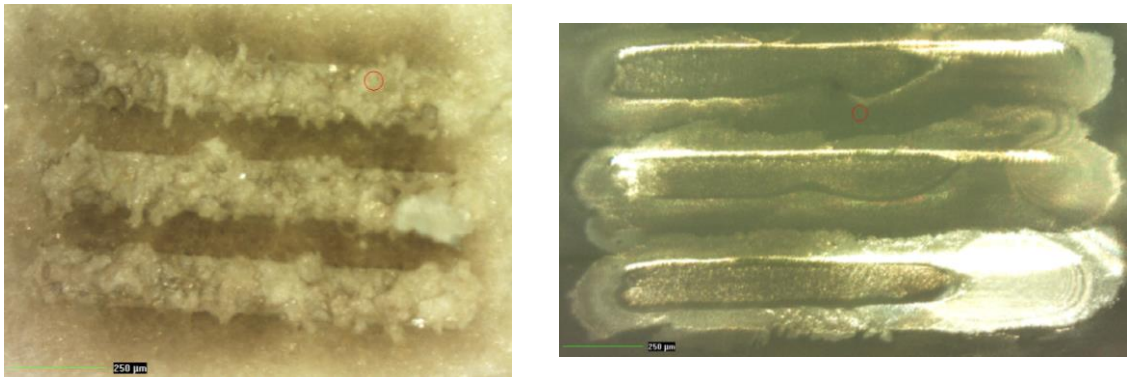

a) **b)**

Figure 15: Ablation craters formed by line scans along the surface of a) a pellet standard and b) a film standard.

Table 3: Parameters used for the ablation of film standards. Ablation was carried out in the Cryostage.

Parameter	LIBS J200
Laser fluence ($J \cdot cm^{-2}$)	14.3
Spotsize (µm)	140
Repetition rate (Hz)	20
Shot count (-)	40
Ablation atmosphere	1 $L \cdot min^{-1}$ argon

Die approbierte gedruckte Originalversion dieser Diplomarbeit ist an der TU Wien Bibliothek verfügbar
The approved original version of this thesis is available in print at TU Wien Bibliothek.
TU Bibliothek Your knowledge hub WIEN

Hence, it was decided to produce polymer films, with the reasons being twofold. On the one hand, an in-house produced film can replicate an industrial polymer film to a certain degree. On the other hand, the used preparation method still enabled the introduction of deuterated benzoic acid into the polymer film matrix. Several sets of standards were produced in order to test different ablation parameters. During this process it became clear that high laser fluences resulted in increased $^{40}Ar^2D^+$ signal. Consequently, the experiments reported from here onwards were conducted with the LIBS J200, because of its higher energy output. Additionally, spots instead of lines were ablated on the films as they did not induce clogging of the transfer line, but also showed greater repeatability. The optimized ablation parameters used for the calibration experiments in 4.2.1 and 4.2.3 are given in Table 3. Once more, the goal was to measure the bulk polymer, which is why the depth of the polymer layer was ablated within a single spot pattern. The standards were ablated in the Cryostage.

4.2.1 Calibration with PI

The foundation of the results shown in this section is a series of 24 individual film standards made by combining 75 mg·g^{-1} polyimide solution in NMP with a mixture of deuterated benzoic acid dissolved in NMP and regular deuterated benzoic acid dissolved in NMP (cf. 3.5.2). The final concentration of deuterated benzoic acid in the film was ~0-113 mg·g^{-1}, corresponding to ~0-9 mg·g^{-1} of added deuterium. These standards were ablated using a total of nine spot patterns, spaced equally across a 1 × 1 mm square.

Signal intensities of ^{13}C and $^{40}Ar^2D^+$ are illustrated in Figure 16 for a standard containing 0 and 9 mg·g^{-1} added deuterium, respectively. Clear differences in $^{40}Ar^2D^+$ signal

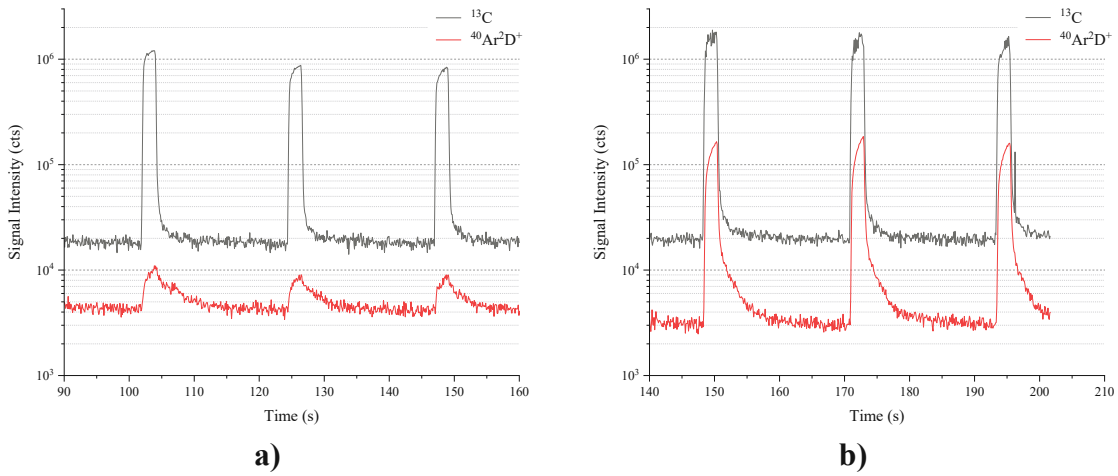

Figure 16: Signal intensities of ^{13}C (black) and $^{40}Ar^2D^+$ (red) for a film standard containing a) no added deuterated benzoic acid and b) approx. 9 mg·g^{-1} added deuterium. For both standards, the signal intensities resulting from three separate spot patterns are shown. Ablation was carried out in the Cryostage.

Die approbierte gedruckte Originalversion dieser Diplomarbeit ist an der TU Wien Bibliothek verfügbar
The approved original version of this thesis is available in print at TU Wien Bibliothek.

are visible, which are larger than observed for the pellet standard with 16 $mg \cdot g^{-1}$ (cf. Figure 11b) right). Thus, during method development signal enhancement was achieved, considering that the signal is now more than an order of magnitude larger than the background. The higher laser fluence boosts ablation rate, which also brings about an increased ^{13}C signal. Furthermore, the fact that the blank standard exhibits an increased $^{40}Ar^{2}D^{+}$ signal supports the claim in 4.1.1 that naturally abundant deuterium contributes to the background during laser ablation, which is enhanced by the higher laser fluence.

For calibration, a different measure of signal processing had to be used. As the produced peak was rather wide and undeniably unstable during the 2 s of ablation, the entire peak including the wash-out phase was integrated to arrive at a region area. The first integration bound was set approx. 0.5 s before ablation and the second bound such that a total of 10 s was integrated. The blank signal without ablation (gas blank) was corrected for by utilizing a 5 s region ahead of every individual ablation pattern.

The calibration curves themselves are illustrated in Figure 17 and Figure 18 for the $^{40}Ar^{2}D^{+}$ region area and the normalized $^{40}Ar^{2}D^{+}$ region area, respectively. Here, normalization plays an even bigger part, which partially results from laser energy differences between patterns (cf. 4.1.1). However, it is important to reemphasize that the in-house produced polymer films only resemble a commercial product in terms of ablation characteristics (when disregarding additives that alter the absorption behavior). Industrial grade polyimide films usually possess a defined layer thickness that is constant on a microscopic scale. The same cannot be said for the fabricated film standards as coffee ring effects occur during the NMP evaporation that cause inhomogeneous film thickness. More often than not, the standard would be thicker at the edges of the silicon wafer compared to the center. If the center was analyzed, less material was ablated and less signal obtained in the ICP-MS. Hence, there were two reasons to correct for different quantities of ablated material by normalizing the $^{40}Ar^{2}D^{+}$ signal to that of ^{13}C.

Despite signal normalization, the standards show larger deviation from the calibration curve with increasing deuterium concentration. No well-founded explanation for this effect, which was visible for the pellet standards too, can be given currently. Conversely, the relative standard deviation (RSD) between ablation patterns on the same standard generally decreases with increasing concentration. In this regard, standards with 9 $mg g^{-1}$ added deuterium exhibit an RSD of 7-14 %, whereas standards with no added deuterium show 23-

Die approbierte gedruckte Originalversion dieser Diplomarbeit ist an der TU Wien Bibliothek verfügbar
The approved original version of this thesis is available in print at TU Wien Bibliothek.

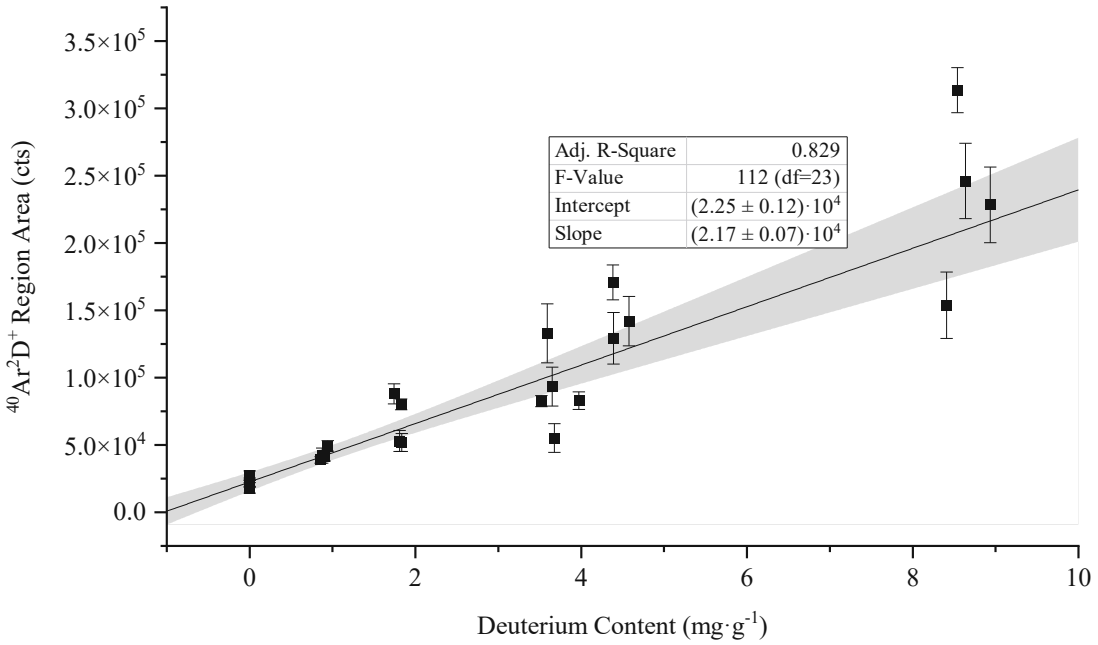

Figure 17: Film standard calibration based on the $^{40}Ar^2D^+$ region area for polyimide. The error bars represent the standard error of nine individual measurements. Ablation was carried out in the Cryostage.

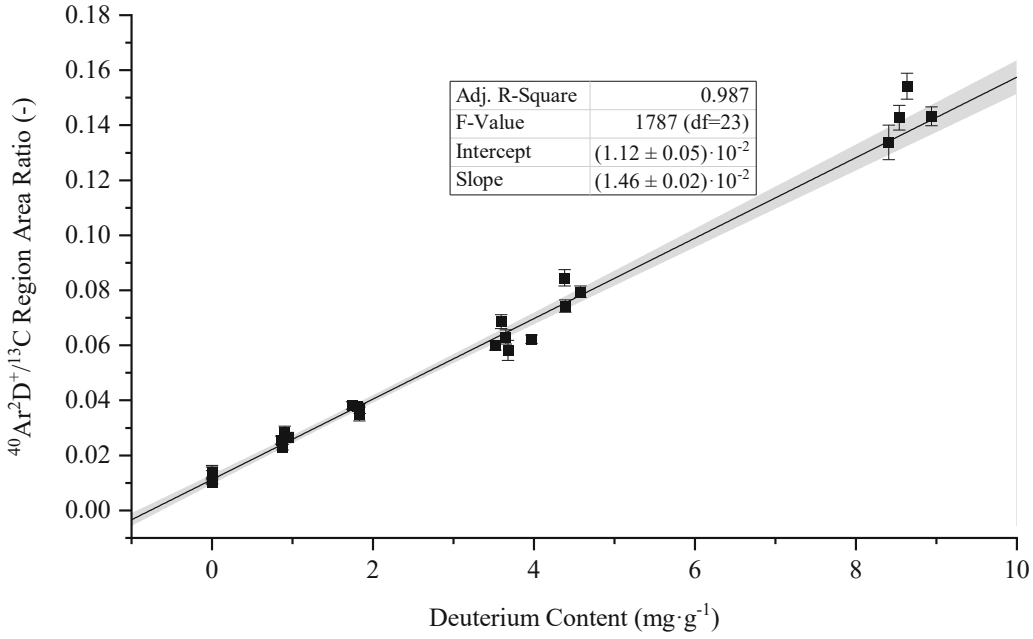

Figure 18: Film standard calibration based on the normalized $^{40}Ar^2D^+$ region area for polyimide. The error bars represent the standard error of nine individual measurements. Ablation was carried out in the Cryostage.

Die approbierte gedruckte Originalversion dieser Diplomarbeit ist an der TU Wien Bibliothek verfügbar
The approved original version of this thesis is available in print at TU Wien Bibliothek.

67 % (based on four standards each). The latter is not surprising, considering that almost no deuterium is present in these standards. Nevertheless, the calibration in Figure 18 based on normalized $^{40}Ar^2D^+$ signal intensity enables quantification of deuterium up to 10 $mg \cdot g^{-1}$, corresponding to concentrations 100 times larger than the natural abundance. As a result, the absorption of deuterium oxide by polyimide film should be detectable when considering that polyimides can take up ~30 mg of water per gram of polymer [40]. If deuterium oxide is absorbed in the same way as regular water, 30 $mg \cdot g^{-1}$ D_2O are equal to 6 $mg \cdot g^{-1}$ deuterium, a value which is covered by the calibration curve.

4.2.2 Influence of the Ablation Atmosphere

It has not been discussed so far, why argon was used as an ablation gas instead of helium, in spite of the improved ablation properties of helium (cf. 2.2.1). Generally, the amount of ablated material is considered to be larger in a helium atmosphere [41,42]. Jacob et al. found that this was also the case for polymers, but the difference between argon and helium atmosphere was minute [43]. However, the initial experiments on the pellet and film standards revealed a surge in both $^{40}Ar^2D^+$ and ^{13}C signal in argon atmosphere, indicating that for these particular standards higher ablation rates were achieved.

In order to validate this, half of the polyimide film standards used for the calibration in the previous chapter were analyzed in both helium and argon. For this purpose, the standards were ablated in the Cryostage with the parameters given in Table 3, but the ablation atmosphere was reduced to 0.6 $L \cdot min^{-1}$ helium or argon. This reduction was necessary to enable ablation helium, since the ICP plasma would become unstable otherwise. The outflow of the Cryostage was mixed with 1 $L \cdot min^{-1}$ argon as a make-up gas using a nebulizer-like contraption so as to attain the same position of the ICP plasma with respect to the sample cone, regardless of the used ablation gas. 1 $L \cdot min^{-1}$ argon flow was chosen as it resulted in a reduced background for $^{40}Ar^2D^+$ without affecting the absolute signal during measurement of a standard with high deuterium concentration.

The calibration curves of measurements in the different ablations atmospheres are shown in Figure 19 and Figure 20. Evidently, higher sensitivity with regards to $^{40}Ar^2D^+$ is achieved when ablating in argon. The slope of the regression curve for argon is thrice as large as that for helium. Note that the $^{40}Ar^2D^+$ signal of the standards with ~9 $mg \cdot g^{-1}$ added deuterium only amounts to a third of the signal observed in the optimized calibration experiments (cf. Figure 17). This can be explained by the different ablation gas flow through

Die approbierte gedruckte Originalversion dieser Diplomarbeit ist an der TU Wien Bibliothek verfügbar
The approved original version of this thesis is available in print at TU Wien Bibliothek.

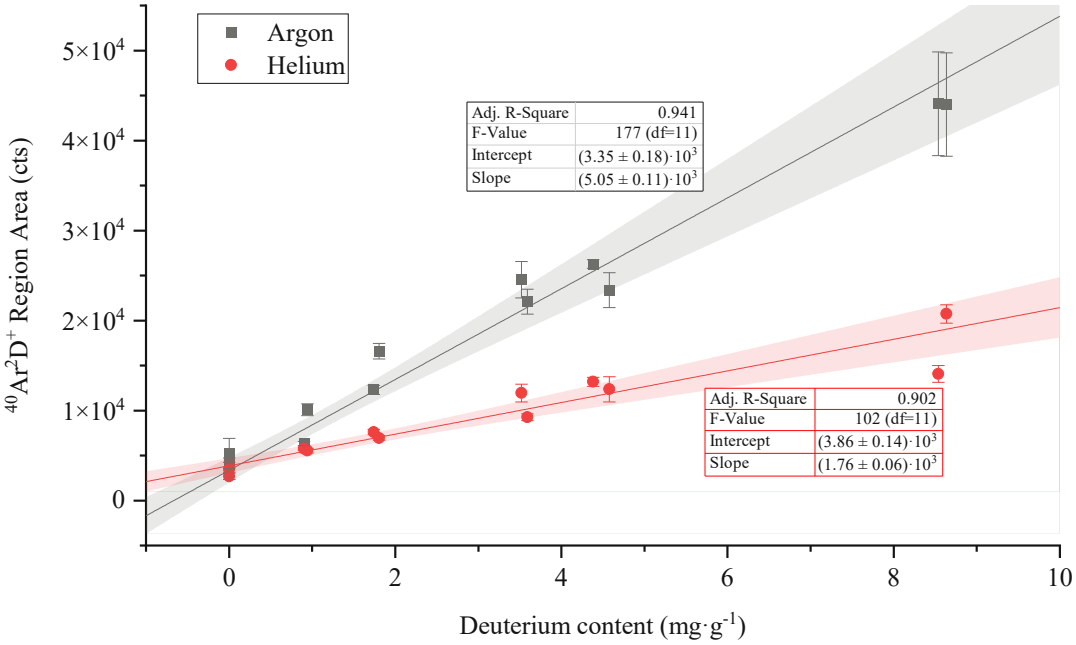

Figure 19: Calibration based on $^{40}Ar^2D^+$ region area in helium (red) and argon atmosphere (black). The error bars represent the standard error of nine individual measurements. Ablation was carried out in the Cryostage.

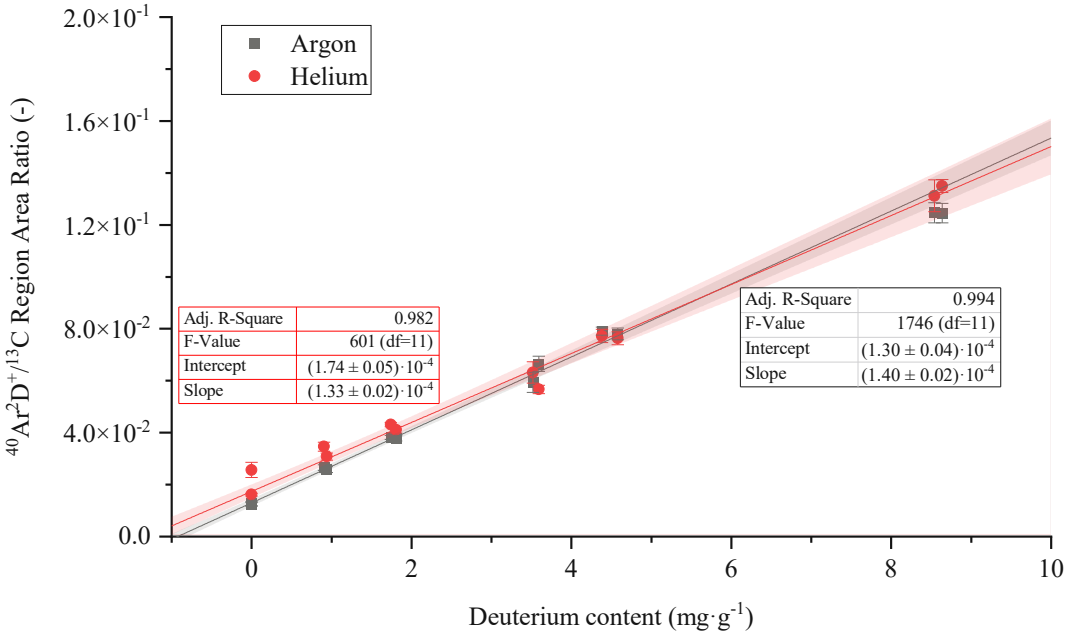

Figure 20: Calibration based on normalized $^{40}Ar^2D^+$ region area in helium (red) and argon atmosphere (black). The error bars represent the standard error of nine individual measurements. Ablation was carried out in the Cryostage.

Die approbierte gedruckte Originalversion dieser Diplomarbeit ist an der TU Wien Bibliothek verfügbar
The approved original version of this thesis is available in print at TU Wien Bibliothek.
TU Bibliothek Your knowledge hub WIEN

the Cryostage (0.6 $L \cdot min^{-1}$ versus 1.0 $L \cdot min^{-1}$) and the alternate experiment setup (addition of make-up gas versus direct injection of sample aerosol).

Besides, it is surprising that normalization to the ^{13}C signal makes the calibration curves for helium and argon almost congruent, as depicted in Figure 20. This would suggest that either the ablation rate in helium is lower or that the argon atmosphere ultimately delivers increased signal intensities in the ICP-MS. Both options are reasonable. In principle, the entire depth of the polymer layer was ablated during these measurements, so ablation rate should not be the deciding factor. However, the high temperature of the laser plasma means that regions beyond the ablation crater can evaporate and contribute to the ICP-MS signal. An in-depth study of the ablation craters in different ablation atmospheres was beyond the scope of this thesis so this influence cannot be disproven. Conceivably, the concentration of argon in the ICP plasma could be crucial for the formation of the $^{40}Ar^2D^+$ ion; hence, using helium as ablation gas would deteriorate the signal. This would not impact the carbon signal though, leading to differences in the calibration curves of the normalized $^{40}Ar^2D^+$ signal between helium and argon. Another feasible explanation are non-identical positions of the ICP plasma when using helium or argon despite using the same mass flow.

4.2.3 Calibration with PMMA

To investigate if calibration of deuterium was also possible in other polymers, film standards were produced from a 75 $mg \cdot g^{-1}$ PMMA solution in NMP. In every other aspect the films were produced in the same way as in 4.2.1 and calibration was performed using the same data treatment. Nevertheless, it has to be mentioned that the PMMA films exhibited even worse coffee stain effects than experienced for polyimide, resulting in a pronounced high-thickness region at the edge of the silicon wafer with the center only being covered by a very thin layer. It was therefore decided to only ablate the edge region by using a 9 x 1 spot pattern equally spaced along a line of 2.4 mm length.

The corresponding calibration curves are depicted in Figure 21 and Figure 22 for the $^{40}Ar^2D^+$ and normalized $^{40}Ar^2D^+$ signal, respectively. Less $^{40}Ar^2D^+$ signal is generated, with the sensitivity of the calibration curve being halved compared to the polyimide calibration in Figure 17. It is not shown here, but since the carbon signal intensity is approximately the same as for polyimide, the normalized $^{40}Ar^2D^+$ signal is decreased, which can be seen by comparing the slope of the regressions in Figure 18 and Figure 22. No explanation for this deviation could be found. Urech and Lippert provide a reasonable explanation by pointing

Die approbierte gedruckte Originalversion dieser Diplomarbeit ist an der TU Wien Bibliothek verfügbar
The approved original version of this thesis is available in print at TU Wien Bibliothek.

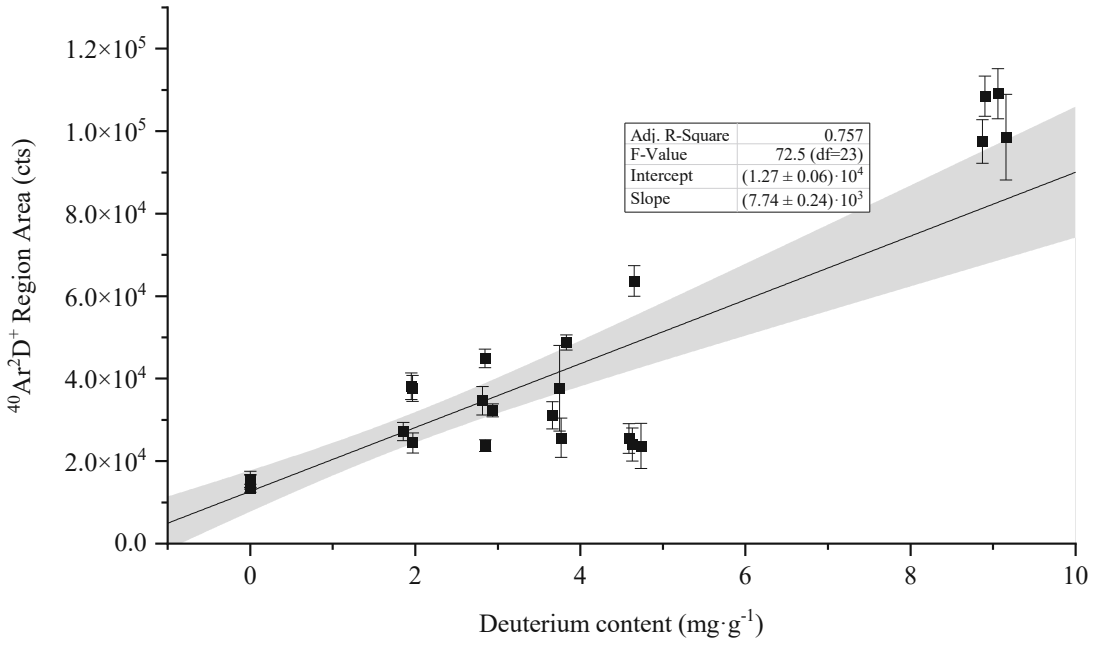

Figure 21: Film standard calibration based on the $^{40}Ar^2D^+$ region area for PMMA. The error bars represent the standard error of nine individual measurements. Ablation was carried out in the Cryostage.

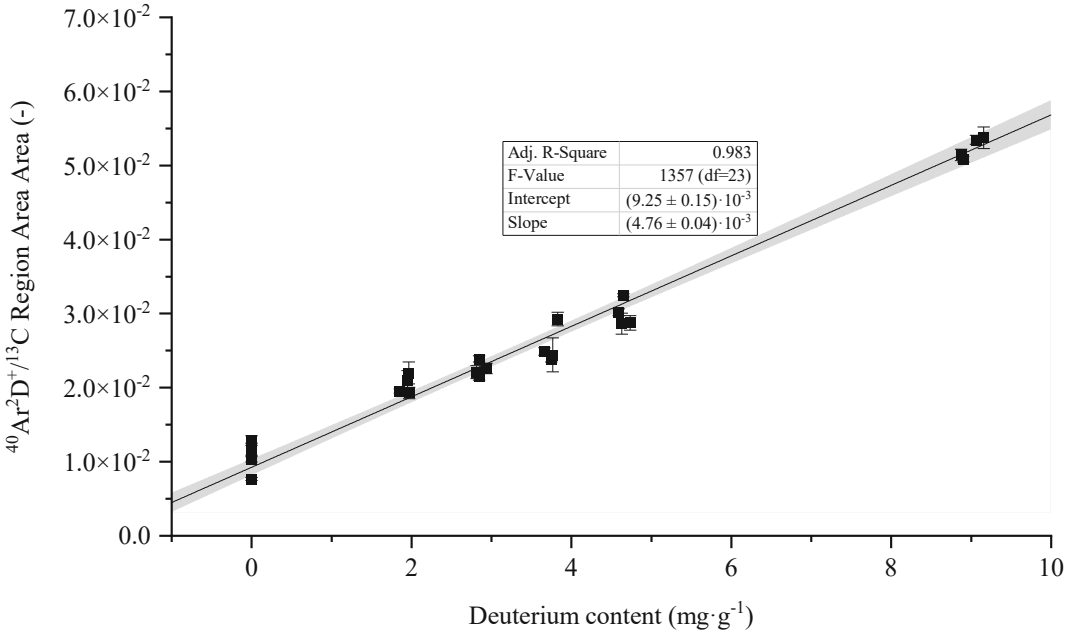

Figure 22: Film standard calibration based on the normalized $^{40}Ar^2D^+$ region area for PMMA. The error bars represent the standard error of nine individual measurements. Ablation was carried out in the Cryostage.

Die approbierte gedruckte Originalversion dieser Diplomarbeit ist an der TU Wien Bibliothek verfügbar
The approved original version of this thesis is available in print at TU Wien Bibliothek.

out that "the ablation of polymers will always be a mixture of photochemical and photothermal reactions, where the ratio between the two is a function of the polymer and the irradiation wavelength." [44] Moreover, the particles generated during the ablation of polyimide and PMMA could very well be dissimilar (e.g., in terms of size distribution), which could lead to distinct degrees of vaporization and atomization in the ICP plasma. In spite of the reduced sensitivity, the normalized $^{40}Ar^{2}D^{+}$ signal intensities still cluster close to the calibration curve, thus substantiating that the method can be used for different polymer types.

4.2.4 Regarding Internal Standardization to Carbon or Platinum

In the previous chapters it was discussed how internal standardization to carbon can correct for different amounts of ablated material between individual ablation patterns. Two reasons for the necessity of internal standardization were given so far:

- deviating laser energy from pattern to pattern despite using the identical ablation patterns (particularly for the LIBS J200 laser) and/or
- inhomogeneous film thickness, i.e., quantity of ablated material from the polymer layer.

In LA-ICP-MS, internal standardization is typically performed by adding known quantities of an element to correct for the variation in sample introduction and ionization efficiency, e.g., "sensitivity drift, matrix effect [*sic*] as well as the difference in ablation yield between samples and reference materials […]." [45] The chosen isotope should have a mass number close to that of the investigated analyte to improve accuracy and precision, considering that a large difference in mass can lead to additional fractionation [46]. Usually, using carbon for normalization could be seen as an imprecise approach, because the exact amount of carbon in the polymer matrix is oftentimes unknown and trace metals typically have high mass. In this case however, carbon is ubiquitous in the standards and can be considered homogeneously distributed since both the polymers and the (deuterated) benzoic acid contain carbon as the major component. Nevertheless, different degrees of atomization could conceivably occur between the carbon in the (deuterated) benzoic acid and the polymer when considering the respective bond strengths, resulting in some sort of fractionation. This is not expected, however, when keeping the high energy of the ICP in mind.

To investigate whether internal standardization to an element not contained in the polymer matrix would deliver better results, platinum was added to the standards in the form of Pt-acac (cf. 3.5.2). The signal intensity of the ^{196}Pt isotope was measured during all experiments involving film standards to investigate possible overlap with the $^{40}Ar^{2}D^{+}$ signal.

Die approbierte gedruckte Originalversion dieser Diplomarbeit ist an der TU Wien Bibliothek verfügbar
The approved original version of this thesis is available in print at TU Wien Bibliothek.
TU Bibliothek Your knowledge hub WIEN

Figure 23 illustrates the ^{13}C, $^{40}Ar^2D^+$ and ^{196}Pt signal of a polyimide film standard containing 0 and 9 $mg \cdot g^{-1}$ deuterium, respectively; the platinum concentration in these films was approx. 0.7 $mg \cdot g^{-1}$. It is evident that the ^{196}Pt signal replicates the ^{13}C signal for the majority of the ablation process and that it also correlates highly with the $^{40}Ar^2D^+$ signal of the standard with the larger deuterium concentration. The main difference between carbon and platinum is the tailing of the peaks. After the ablation pattern is completed, the ^{196}Pt signal requires ~1.5 s to return to the baseline, whereas the ^{13}C signal requires more than 3 s. Without further proof, it is assumed that the larger tailing for carbon occurs, because it is partially transported to the ICP-MS as a gas (cf. 4.1.2 and [39]), whereas platinum is contained in the aerosol particles that are then atomized in the ICP.

It is important to reemphasize that the contribution of gaseous carbon is deemed to restrict the use of carbon as internal standard as discussed by Makino and Nakazato [39]. However, for this topic it could be advantageous since the $^{40}Ar^2D^+$ ion exhibits even larger tailing that increases with deuterium concentration in the standards, which would indicate that deuterium is partially transported as a gas too. Hence, internal standardization to carbon could cover for the portion of gaseous deuterium released during ablation, whereas ^{196}Pt cannot. In fact, calibration curves based on the $^{40}Ar^2D^+$ signal normalized to ^{13}C show improved linear fits compared to the signal normalized to ^{196}Pt. Moreover, when measuring real samples the introduction of platinum is not possible. Hence, normalization to carbon is the preferred option either way.

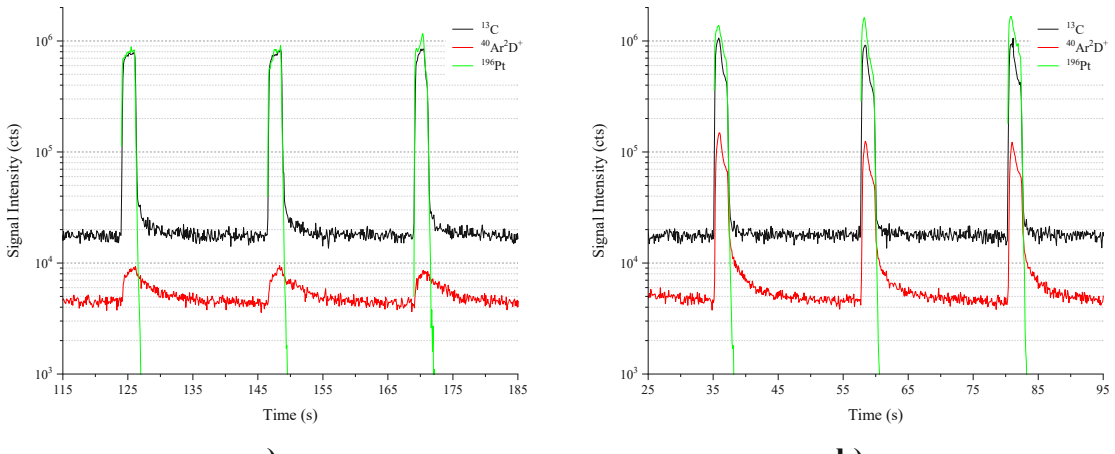

Figure 23: Comparison of ^{13}C (black), $^{40}Ar^2D^+$ (red) and ^{196}Pt (green) signal intensities for a standard containing a) no added deuterated benzoic acid and b) approx. 9 $mg \cdot g^{-1}$ added deuterium. For both standards, the signal intensities resulting from three separate spot patterns are shown. Ablation was carried out in the Cryostage.

Die approbierte gedruckte Originalversion dieser Diplomarbeit ist an der TU Wien Bibliothek verfügbar
The approved original version of this thesis is available in print at TU Wien Bibliothek.

4.3 On the Bonding of Deuterium in Standards and Samples

Up until now, results were presented for specimens containing deuterium that is bound chemically to a matrix component. In the standards, this component is deuterated benzoic acid, which roughly contains 79.2 $mg \cdot g^{-1}$ deuterium bound to the carbon atoms of the aromatic benzene ring by covalent bonds. The dissociation energy of the C-H bonds in benzene is 110.9 ± 2 $kcal \cdot mol^{-1}$ [47,48]. No literature reference could be found for benzoic acid, but it is reasonable to assume that this value is approximately equal in benzoic acid and, more importantly, that it is close to the bond energy of the C-D bond in deuterated benzoic acid.

In contrast, water absorption by polymers relies on "water dissolution in a superficial polymer layer […] and water diffusion into the sample core" [49]. The former occurs instantaneously, while the latter requires a chemical potential gradient. "Water solubility is closely related to the content of polar groups in the polymer and to the strength of the hydrogen bonds that they are able to establish with water molecules." [49] Diffusion, on the other hand, is mainly contingent upon the free volume of a polymer, i.e., the amount of space between polymer chains. Hence, two different types of water molecules are present in the polymer after absorption: "mobile (free) molecules diffusing through the sample and bound (immobile) molecules temporarily delayed at [polar moieties of the polymer] by hydrogen bonds." [49] At equilibrium, significantly more bound than mobile water molecules are present. However, it is important to note that bound water does not signify permanently bound. Complexes formed between the polar groups of the polymer and the bound water portion have a finite lifetime and therefore water is readily bound and unbound constantly. [49]

Regarding bond strength, hydrogen bonds lie between strong covalent bonds (100-200 $kcal \cdot mol^{-1}$) and weak van-der-Waals bonds (0.1-1 $kcal \cdot mol^{-1}$). In a hydrogen bond of the general structure X–H···Y, the hydrogen atom acts as a link between an electronegative atom X (e.g., oxygen or nitrogen) and a proton acceptor Y. This Y can either be an electronegative region, e.g., electronegative atoms, or a region of electron excess, such as π electrons. As a consequence of hydrogen bonding, the covalent X-H bond is weakened due to elongation, while the formed H···Y bond – that is, the actual hydrogen bond – can even develop covalent character, especially if the hydrogen bond is strong. Bond strengths can assume values of 0.1-60 $kcal \cdot mol^{-1}$ and are highly correlated to the bonding partners and geometry involved. However, hydrogen bond energies above >25 $kcal \cdot mol^{-1}$ are only observed for particular cases, e.g., for the $[FHF]^-$ anion (61.1 $kcal \cdot mol^{-1}$). [50]

Die approbierte gedruckte Originalversion dieser Diplomarbeit ist an der TU Wien Bibliothek verfügbar
The approved original version of this thesis is available in print at TU Wien Bibliothek.
TU Bibliothek Your knowledge hub WIEN

In synthetic polymers, hydrogen bonds can act as cross-linkers by connecting polymer chains. For instance, polyamides, such as Nylon 66, form hydrogen bonds between the N-H- and C=O-parts of two separate amide groups. In fact, a large majority of the N-H-groups in polyamides are involved in hydrogen bonds at room temperature [51]. The hydrogen bond strength for these cases is in the region of 8-12 $kcal \cdot mol^{-1}$ [51]. When considering the interaction of polymer and water in this regard, hydrogen bonds between water and N-H-, O-H- or C=O groups of the polymer (side) chains are feasible options for most polymers. The approximate strength of the relevant hydrogen bonds are given in literature as follows: 7 $kcal \cdot mol^{-1}$ for O-H···N, 5 $kcal \cdot mol^{-1}$ for O-H···O, and 2 $kcal \cdot mol^{-1}$ for N-H···O [52]. However, water can be bound to the polymer by multiple hydrogen bonds too. For instance, Lee, Chang and Ju found that water forms three hydrogen bonds in a sub-surface region and two hydrogen bonds in the surface region of a PMMA film by interaction with the carbonyl groups [53]. All things considered, for the system polymer/water, hydrogen bonds are expected to be of moderate strength (<15 $kcal \cdot mol^{-1}$) at most.

Consequently the difference in bond strength of deuterium is almost an order of magnitude between samples and standards. The deuterium bound as (mobile) D_2O indeed requires a smaller chemical potential gradient to desorb from the polymer, which can be established by increasing the temperature, for instance. Alternatively, the partial pressure of D_2O in the surrounding atmosphere could be reduced, such that the water diffuses from the bulk to the surface, where it is then be desorbed. In contrast, breaking of the covalent C-D bond demands energies that would suffice for combustion of the compound.

4.4 Qualitative Comparison of Water Absorption by Polyimides from Liquid D_2O

After briefly discussing the fundamentals of water absorption by polymers, the question remains whether this absorption, or more precisely, the absorption of deuterium oxide can actually be detected with LA-ICP-MS. To test this, the industrial polyimides PI 1, PI 2 and PI 3 were subjected to deuterium oxide. Initially, samples of the polyimides were submerged in liquid deuterium oxide since the absorption of water from the liquid phase is supposed to be higher than that from the gas phase (~30 $mg \cdot g^{-1}$ compared to ~12 $mg \cdot g^{-1}$) [40].

4.4.1 Sample Treatment and Importance of the Cryostage

The samples were treated as set out in 3.6 and then analyzed in the Cryostage, though this was the first time that cooling of the samples actually took place. Cooling of the samples

Die approbierte gedruckte Originalversion dieser Diplomarbeit ist an der TU Wien Bibliothek verfügbar
The approved original version of this thesis is available in print at TU Wien Bibliothek.

was deemed necessary considering that dealing with samples, which contained absorbed heavy water, consistently lead to large backgrounds for $^{40}Ar^{2}D^{+}$ in many previous experiments. As a result, the signal-to-background ratio (SBR) was compromised. The hypothesis was that the deuterium oxide desorbs due to the large difference in partial pressure of D_2O in the sample and the dry argon gas atmosphere of the ablation cell/Cryostage. Previously, the Cryostage was used to analyze the film standards in order to eliminate inconsistencies in experiment setup between standards and samples – e.g., the flow regime – with the sole intention to maybe apply the calibration data of the polyimide films to the samples.

The purpose of the experiments was to observe the $^{40}Ar^{2}D^{+}$ signal of samples that were submerged in deuterium oxide and, as a reference, samples that were submerged in regular, deionized water as well as samples that were not submerged at all. For laser ablation, the same parameters as for the film standards were used (cf. Table 3). ^{13}C and $^{40}Ar^{2}D^{+}$ signal intensities of a PI 1 sample submerged in regular and heavy water, respectively, are depicted in Figure 24. For the sample submerged in regular water, the $^{40}Ar^{2}D^{+}$ signal amounts to 2,000-3,000 counts atop a background of 3,000 counts. In contrast, the sample submerged in D_2O exhibits an $^{40}Ar^{2}D^{+}$ signal of 40,000-50,000 counts atop a comparatively large background of 10,000 counts.

This background, that is almost an order of magnitude larger than experienced for the film standard calibration (cf. Figure 16), is best explained by looking at Figure 25. In the beginning of the measurement of a sample submerged in heavy water, the Cryostage is open

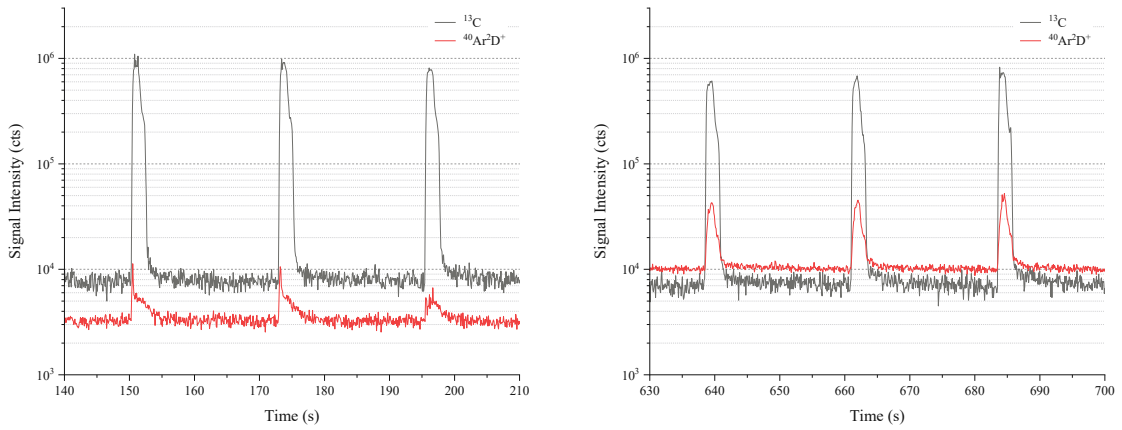

Figure 24: Signal intensities for PI 1 samples submerged in a) deionized water and b) D_2O. For both samples, the signal intensities resulting from three separate spot patterns are shown. Ablation was carried out in the Cryostage operated at -12 °C.

Die approbierte gedruckte Originalversion dieser Diplomarbeit ist an der TU Wien Bibliothek verfügbar
The approved original version of this thesis is available in print at TU Wien Bibliothek.

to allow for sample introduction. Hence, the sample cavity is solely flushed with argon, whilst no transport of material to the ICP-MS takes place. As soon as the Cryostage is sealed gas-tight, the dry argon carrier gas can exit the Cryostage through the opening connected to the ICP. Simultaneously, the background of ^{13}C and $^{40}Ar^2D^+$ change. In the case of carbon this is caused by residual carbon species of the surrounding atmosphere (CO, CO_2, etc.) and an equilibrium background intensity is assumed after approx. 100 s. For $^{40}Ar^2D^+$, the background amounts to 20,000 counts and seems to be decreasing very slowly and exponentially over time. The large timespan and the fact, that no equilibrium was established, renders it highly unlikely that the air introduced during sample exchange effectuates this background.

All things considered, the only feasible explanation for this phenomenon is the desorption of deuterium oxide from the sample. This is backed up by two further observations. On the one hand, the background increases as soon as cooling by the Cryostage is turned off, as can be seen in Figure 25 by the $^{40}Ar^2D^+$ signal increase from 800 s onwards. This coincides with the fact that desorption rates are dependent on temperature, where an increased temperature causes higher desorption. On the other hand, the background appears exclusively for samples that were submerged in heavy water, not for samples submerged in regular water. Even though this impedes the practicability of water absorption measurements, a background at m/z 42 that appears to be related to desorption, can be interpreted as a proof that the signal for $^{40}Ar^2D^+$ does in fact represent deuterium. Moreover, this shows that deuterium is at least partially transported as a gas to the ICP-MS.

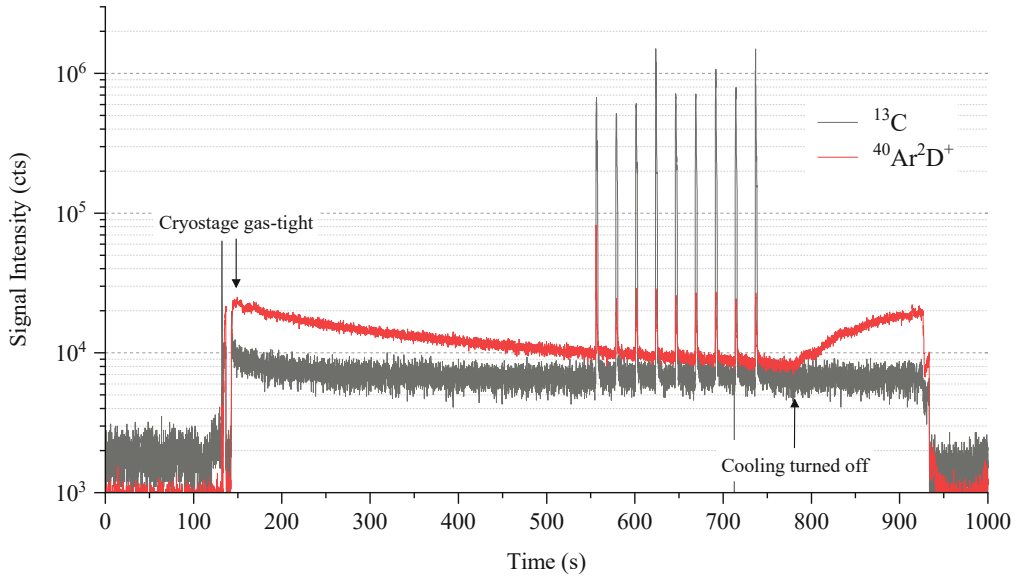

Figure 25: Exemplary ^{13}C (black) and $^{40}Ar^2D^+$ (red) signal intensity trend during measurement of a PI 3 sample submerged in deuterium oxide, where the cooling was turned off after the ablation patterns. Ablation was carried out in the Cryostage operated at -12 °C.

Die approbierte gedruckte Originalversion dieser Diplomarbeit ist an der TU Wien Bibliothek verfügbar
The approved original version of this thesis is available in print at TU Wien Bibliothek.
TU Bibliothek Your knowledge hub WIEN

4.4.2 Comparison of the Polyimides

Turning the attention back towards the laser ablation process, it has to be pointed out that the samples submerged in D_2O were ablated only after the background had decreased to approx. 10,000 counts. This was done for consistency in terms of SBR, because the different samples provided distinct onsets of the high background at m/z 42. Some samples even exhibited a background of 80,000 counts after ensuring gas-tightness of the Cryostage. Conceivably, this could be the result of residual water adsorbed on the sample, which was not wiped off sufficiently before freezing the samples. This adsorbed water would have not been taken up by the polymer, but rather remained on the surface due to surface tension, providing additional amounts of water that would then evaporate in the Cryostage.

To compare the three polyimide types, the following samples were analyzed: one sample not submerged at all, one sample submerged in regular water as well as three samples submerged in deuterium oxide. Even though the industrial polyimides have a homogeneous film thickness, internal standardization to ^{13}C was still necessary so as to correct for inconsistent laser energies between patterns. The obtained normalized $^{40}Ar^2D^+$ signal intensities are illustrated in Figure 26, where the region area of the peaks was used for data evaluation (cf. 4.2.1). When comparing samples that were not submerged to samples that were submerged in D_2O, a noticeable boost in signal intensity can be observed. The absolute $^{40}Ar^2D^+$ signal intensity varied between 30,000 and 50,000 counts for the D_2O samples, whereas non-submerged samples provided a signal of ~2,000 counts. Hence, it can be concluded that the absorption of deuterium oxide did indeed take place.

It is important to emphasize that the goal again was to achieve bulk measurements by ablating the entire polymer layer. Local differences in water absorption could feasibly contribute to signal variations, leading to the large error bars in Figure 26. They appear larger for the submerged samples due to the scale, but the RSD values (7-35 %) are similar to those of the native samples (10-36 %). Consequently, other contributions to the standard error are realistic. For instance, the sample preparation, that comprises of many steps where water could desorb from the sample or attach to the surface uncontrollably, seems to be crucial. This is supported by the fact that film standards with a comparable normalized $^{40}Ar^2D^+$ signal intensity generally exhibit a more reproducible RSD of 10-21 % (based on four polyimide standards with 1.8 $mg \cdot g^{-1}$, cf. 4.2.1). Moreover, this would explain the differences between the individual samples of the same polyimide type submerged in heavy water, where one sample of every type delivers significantly deviating normalized signal intensity.

Die approbierte gedruckte Originalversion dieser Diplomarbeit ist an der TU Wien Bibliothek verfügbar
The approved original version of this thesis is available in print at TU Wien Bibliothek.
TU Bibliothek Your knowledge hub WIEN

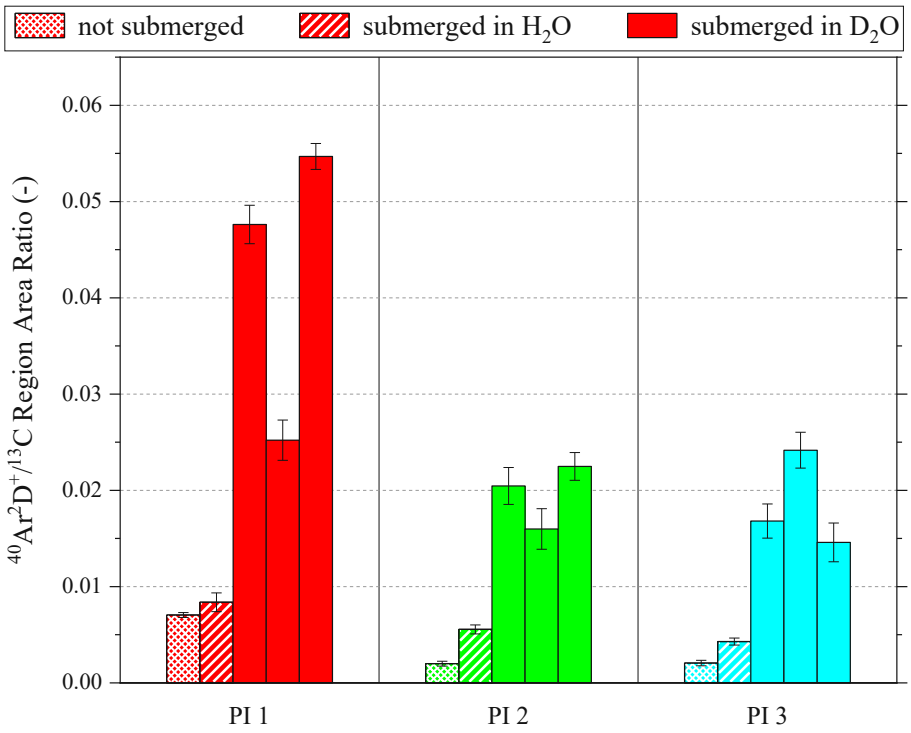

Figure 26: Normalized $^{40}Ar^2D^+$ signal of the industrial polyimides PI 1 (red), PI 2 (green) and PI 3 (petrol blue). The leftmost bar represents a sample that was not submerged at all. The bar second to the left represents a sample submerged in regular water. The remaining bars represent samples that were submerged in D_2O. The error bars represent the standard error of nine individual measurements.

Nevertheless, qualitative differences between the polyimide types can be seen. PI 1 appears to exhibit increased water absorption compared to PI 2 and PI 3. In fact, a divergence in absorption behavior was expected since PI 1 is produced in a different way than the other two. Curiously, for PI 2 and PI 3 the samples submerged in regular water show notably increased normalized $^{40}Ar^2D^+$ signal intensity. It is not clear what causes this effect, especially because it is not observed for PI 1. Feasibly, the absorption of regular water could shift the deuterium content in the analyzed volume, but this should also occur for PI 1. Alternatively, the absorbed water could alter the surface in such a way, that ablation is enhanced, e.g., by increasing the absorptivity of the laser photons or changing the roughness of the surface. However, this should affect PI 1 too and would be compensated for by signal normalization to ^{13}C. All in all, the results have to be treated with caution when considering that the experiments were only performed once.

In principle, the calibration data, that was obtained from the polyimide film standards, could be used to quantify the absorption of D_2O. Performing this for the polyimide samples by averaging every ablation pattern on samples of the same type would yield the following results: 105 ± 10 mg·g^{-1} for PI 1; 29 ± 4 mg·g^{-1} for PI 2; 26 ± 5 mg·g^{-1} for PI 3.

Die approbierte gedruckte Originalversion dieser Diplomarbeit ist an der TU Wien Bibliothek verfügbar
The approved original version of this thesis is available in print at TU Wien Bibliothek.

This does correspond to order of magnitude given in literature [40,54]. However, using the calibration data for samples is deemed inappropriate as discussed in the following:

- the background during ablation at m/z 42 and 13 changes over time and as a consequence, comparison of samples and film standards is inappropriate;
- the sample preparation is prone to inconsistencies, e.g., loss of D_2O due to desorption during sample introduction; hence, the normalized $^{40}Ar^2D^+$ signal intensity differs between samples of the same polyimide type.

Therefore, the absorption of water by the polymer films could only be studied qualitatively as improvements in sample handling are imminent to increase reproducibility. For example, D_2O could be introduced in gaseous form, leading to absorption in a more consistent manner.

4.5 Concluding Remarks Regarding the Background at m/z 42

Principally, the calibration curve gathered for the film standards could be extrapolated until it meets the abscissa. The corresponding value would then represent the mixed deuterium content of the regular benzoic acid and the polymer. The requirement for this to be true would be that the only contribution to the background at mass 42 is the deuterium in the matrix. If extrapolation is performed for the polyimide film standards, the corresponding deuterium concentration would be ~0.8 $mg \cdot g^{-1}$, which is eight times larger than the natural abundance (cf. [14]). Clearly, the above stated requirement is not fulfilled.

Until now it remains unclear, what constitutes the background at m/z 42 during ablation. Besides the naturally abundant deuterium there apparently are other sources, which could not be identified in this thesis. Viable contributions at this mass are other combined argon/hydrogen species, calcium contaminations and molecular ions deriving from the polymer. In principle, the formation of polyatomic ions in the ICP is not restricted to two individual atoms; hence, $^{40}Ar^1H_2^+$ could interfere with $^{40}Ar^2D^+$. However, Galbács et al. have disregarded such contributions since the produced ion is very unstable [15]. A calcium background could be disproven for the pellet standards (cf. 4.1.1), which was reaffirmed for the film standards as seen in Figure 27. Though intensities for m/z 43 and 48 could be observed, the isotope ratios differed substantially from the natural abundance of the isotopes. In fact, the background that occurs during ablation at mass 43 is most likely a molecular ion of the polymer, e.g., C_3H_7. It shows the same signal intensity for all standards regardless of deuterium concentration and exhibits larger SBR than mass 42 for a standard containing no deuterium, which contradicts the natural abundance ratios.

Die approbierte gedruckte Originalversion dieser Diplomarbeit ist an der TU Wien Bibliothek verfügbar
The approved original version of this thesis is available in print at TU Wien Bibliothek.

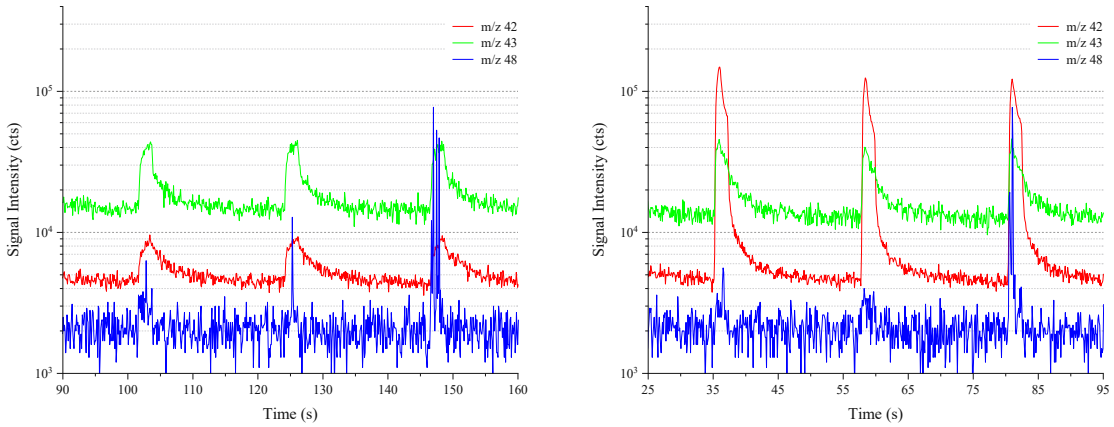

Figure 27: Comparison of the signal intensities at mass 42 (red), 43 (green) and 48 (blue) for film standards. For this figure the signal intensities of standards with a) 0 and b) 9 mg·g^{-1} added deuterium were plotted.

Die approbierte gedruckte Originalversion dieser Diplomarbeit ist an der TU Wien Bibliothek verfügbar
The approved original version of this thesis is available in print at TU Wien Bibliothek.

5. Conclusion and Outlook

This thesis intended to achieve the analysis of deuterium in solid samples using LA-ICP-MS with the prospect of measuring the water uptake by different polymer films. Due to several limitations, detecting deuterium by itself is usually not possible in ICP-MS, which is why Galbács et al. proposed the utilization of polyatomic ions, which are formed in the ICP plasma [15]. For this specific topic, $^{40}Ar^{2}D^{+}$ was assumed to form in sufficient amounts such that high signal intensities are obtained, allowing for qualitative and even quantitative deuterium analysis in polymer matrices.

Indeed, the adoption of the approach by Galbács et al. was a resounding success. Several experiments conducted on pellet standards (containing deuterated benzoic acid) demonstrated that analyzing deuterium by detecting the $^{40}Ar^{2}D^{+}$ ion is possible, whereby lasers with a wavelength of 213 and 266 nm could be used. However, it was clear that pellets were not suitable as a standard for polymer films. Both ablation behavior and amount of ablated material were too dissimilar to reasonably compare standards and film samples. Hence, matrix-matched thin film standard were produced that would mimic industrial film samples at least in ablation characteristics (disregarding additives that alter absorptivity of the polymer). By combining a polymer matrix with regular and deuterated benzoic acid, standards were produced that delivered large LA-ICP-MS signal intensities. After optimization, the signal at m/z 42 was an order of magnitude larger than the background for film standards containing 9 $mg \cdot g^{-1}$ added deuterium.

This even allowed for quantification. The raw $^{40}Ar^{2}D^{+}$ signal exhibited a clear upwards trend corresponding to the increase in deuterium concentration. However, because the amount of ablated material varied from pattern to pattern, inconsistent signal intensity was obtained. Two reasons for this were explained: inhomogeneous thickness of the film standards and deviating laser energy. Internal standardization of the $^{40}Ar^{2}D^{+}$ signal was discussed for ^{13}C and ^{196}Pt. Normalization significantly improved the standard error of individual ablation patterns on an individual standard. As a consequence, the linear regression of the normalized $^{40}Ar^{2}D^{+}$ signal intensity data exhibited a notably narrower confidence band, enabling quantification in a region of 0-10 $mg \cdot g^{-1}$ deuterium. Moreover, it was argued that internal standardization to ^{13}C is beneficial compared to the addition of an element such as platinum, since carbon is the major component in polymers, is homogeneously distributed and can also account for gaseous species.

Die approbierte gedruckte Originalversion dieser Diplomarbeit ist an der TU Wien Bibliothek verfügbar
The approved original version of this thesis is available in print at TU Wien Bibliothek.

Literature suggests that ablation rates are enhanced by using helium as an ablation atmosphere compared to argon [41-43]. However, preliminary experiments indicated that argon improved both the $^{40}Ar^{2}D^{+}$ and ^{13}C signal intensity in this case. In order to compare the ablation gases, 12 film standards were ablated with the same laser ablation and ICP-MS parameters in helium and argon atmosphere. The results proved that the $^{40}Ar^{2}D^{+}$ and ^{13}C signals were augmented in argon. No clear explanation for this circumstance could be found, though it is assumed to be a result of distinct ablation behaviors causing different amounts of material being ablated. Furthermore, the applicability of the film standard preparation method to different polymers was investigated. The comparison of polyimide and PMMA as matrix revealed distinct sensitivities in the polymers: PMMA resulted in decreased absolute and normalized $^{40}Ar^{2}D^{+}$ signal intensities, though calibration was still viable. Hence, the standard preparation method can also be used for other polymers.

All in all, the quantification was achieved successfully for deuterium that is bound covalently to a polymer matrix component, that is, the deuterated benzoic acid. For water absorption, i.e., the absorption of D_2O via hydrogen bonds with the polymer, investigations proved to be more complicated. It was shown that, if polyimide samples are submerged in D_2O, they indeed absorb the liquid considering that submerged samples presented with a significantly increased normalized $^{40}Ar^{2}D^{+}$ signal in relation to native samples. Furthermore, three different industrial polyimide films were tested, where PI 1 exhibited more than double the normalized signal intensity compared to the PI 2 and PI 3. Additionally, it is important to highlight that cooling of samples submerged in D_2O with the Cryostage is indispensable so as to decrease desorption of the heavy water from the surface and therefore the background at m/z 42. This was confirmed by the observation that increased backgrounds only appeared for samples submerged in D_2O, but not in regular water. Furthermore, turning off the cooling of the Cryostage caused the background to surge, suggesting that the desorption rate increases with temperature as is usually the case for desorption.

There is certainly still room for improvements, especially in terms of standard preparation and sample handling. It was mentioned above that signal normalization is in part required to compensate for the inhomogeneous film thickness of the standards. To eliminate this influence, the standards could be produced via spin-coating, for instance, which should level the surface at least on a microscopic scale. Another aspect is the occurrence of coffee stain effects that appear during the production of the film standards when the solvent is evaporated. Many different ways of mitigating this effect are proposed in literature, such as

Die approbierte gedruckte Originalversion dieser Diplomarbeit ist an der TU Wien Bibliothek verfügbar
The approved original version of this thesis is available in print at TU Wien Bibliothek.
TU Bibliothek Your knowledge hub WIEN

evaporation in an alcohol atmosphere [55], reducing the surface tension with surfactants [56] or in-situ gelation of monodisperse materials [57]. With regards to internal standardization, it is important to point out that platinum is not an ideal choice when considering the difference in mass. Employing a beryllium (for hydrogen itself) or scandium compound (for the $^{40}Ar^{2}D^{+}$ ion) would conceivably improve precision compared to platinum as the mass bias between analyte and standard is reduced [45,46].

The sample preparation procedure is very prone to unintended desorptive losses of D_2O, but also to the analysis of water that is merely stuck to the surface due to surface tension and not actually absorbed by the polymer film. As a result, the normalized $^{40}Ar^{2}D^{+}$ signal intensity deviated considerably from sample to sample, despite being the same polyimide type. Due to these variations it is currently not feasible to apply the deuterium calibration data (gathered from the film standards) to the polyimide samples. The absorption of D_2O via the gas phase may reduce the deviations that occur as a result of inconsistent sample preparation as they were experienced for submersion in liquid D_2O. Work on this is still ongoing, but was not included in this thesis due to time constraints.

In this thesis, solely bulk measurements of standards and samples were performed. On the contrary, imaging is an application of LA-ICP-MS, where the analyte distribution across the sample surface is determined. If the distribution is measured along the depth of a sample, the process is called depth profiling. Spatial resolution of imaging and depth profiling analyses with LA-ICP-MS is indirectly proportional to the ablated area and depth, respectively. The spotsize of the laser beam determines the ablated area. However, it also directly affects the ablated volume and in turn the signal intensity obtained in the ICP-MS. In principle, if enhanced spatial resolution is desired for imaging, the spotsize has to be reduced, which in turn decreases sensitivity [58]. The same applies for depth profiling, though the ablated depth is dependent on laser fluence and the number of laser shots per pattern. More generally, high signal intensity for small quantities of ablated sample is desirable for imaging and depth profiling.

Currently, large amounts of ablated material are required to achieve sufficient $^{40}Ar^{2}D^{+}$ signal intensity. In accordance with the results from the pellet standards, the high laser fluences of the LIBS J200 laser notably augmented the $^{40}Ar^{2}D^{+}$ signal. It is still open to debate whether this is a consequence of increased ablation rate or enhanced bond breaking. Either way, the presently obtained signal intensities impair the spatial resolution capabilities

Die approbierte gedruckte Originalversion dieser Diplomarbeit ist an der TU Wien Bibliothek verfügbar
The approved original version of this thesis is available in print at TU Wien Bibliothek.
TU Bibliothek Your knowledge hub WIEN

of the developed approach. Hence, the influence of laser fluence has to be investigated in more detail for lower ablation depths as opposed to the ablation of the entire polymer layer so as to achieve depth profiling, for instance.

Achieving spatial resolution would unlock applications where the influence of moisture on polymer degradation is of interest. For instance, polycarbonates undergo hydrolytic degradation, where carbonate links between the repeating units are broken and O-H end groups form [59]. In polyimides, hydrolysis results in the cleavage of the C-N bond in the imide group [60]. Polyamides are prone to hydrolysis too, but a subsequent polymerization reaction can occur, which links the cleaved amine and acid groups back together [61,62]. Hydrolytic "degradation is typically undesirable as it may have a dramatic effect on the service life, color, mechanical, and thermal properties of the polymer." [62] All in all, it can be concluded from the aforementioned examples that moisture has a significant impact on polymeric materials, especially if the polymers include polar groups, which are susceptible to hydrolysis or form hydrogen bonds. As indicated in the introduction, analyzing the water absorption locally would provide vital information for the semiconductor and microelectronics industry. For instance, if a microchip is encapsulated by a polymer, but the polymer layer is permeable for water, fatigue due to corrosion is inevitable. Depth profiling of a polymer film subjected to gaseous D_2O would allow for investigations on the required film thickness to prevent corrosion in the long term or, more generally, which polymer type is more suitable for a specific application environment.

Die approbierte gedruckte Originalversion dieser Diplomarbeit ist an der TU Wien Bibliothek verfügbar
The approved original version of this thesis is available in print at TU Wien Bibliothek.

Bibliography

[1] Rydz, J.; Opálková Šišková, A.; Zawidlak-Węgrzyńska, B.; et al. Chapter 1 - High-performance polymer applications for renewable energy. In *Nano Tools and Devices for Enhanced Renewable Energy*, Devasahayam, S., Hussain, C. M. Eds.; Elsevier, 2021; pp 3-26.

[2] Rusli, A.; Othman, M. H.; Ku Marsilla, K. I. Plastics in High Heat Resistant Applications. In *Encyclopedia of Materials: Plastics and Polymers*, Hashmi, M. S. J. Ed.; Elsevier, 2022; pp 200-215.

[3] ASTM International. *Standard Test Method for Water Absorption of Plastics*. 2018. Available at: https://www.astm.org/d0570-98r10e01.html (accessed 28.10.2022).

[4] Kusoglu, A.; Weber, A. Z. New Insights into Perfluorinated Sulfonic-Acid Ionomers. *Chemical Reviews* **2017**, *117* (3), 987-1104. DOI: 10.1021/acs.chemrev.6b00159 (acccessed 27.10.2022).

[5] Brack, H.-P.; Scherer, G. G. Modification and characterization of thin polymer films for electrochemical applications. *Macromolecular Symposia* **1998**, *126* (1), 25-49. DOI: 10.1002/masy.19981260105 (acccessed 27.10.2022).

[6] Borup, R.; Meyers, J.; Pivovar, B.; et al. Scientific Aspects of Polymer Electrolyte Fuel Cell Durability and Degradation. *Chemical Reviews* **2007**, *107* (10), 3904-3951. DOI: 10.1021/cr0501821 (acccessed 27.10.2022).

[7] Bowden, M. J. Polymers for Electronic and Photonic Applications. In *Electronic and Photonic Applications of Polymers*, Advances in Chemistry, Vol. 218; American Chemical Society, 1988; pp 1-73.

[8] DIN EN ISO 62:2008-05, Kunststoffe – Bestimmung der Wasseraufnahme (ISO 62:1999).

[9] ASTM Standard D570, 1998e1 (2010), "Standard Test Method for Water Absorption of Plastics," ASTM International, West Conshohocken, PA, 2003, DOI: 10.1520/D0570-98R10E01, www.astm.org.

[10] Mitchell, J. Methods for the determination of water in polymers. *Analytica Chimica Acta* **1976**, *81* (2), 231-263. DOI: 10.1016/S0003-2670(01)82024-9 (acccessed 03.11.2022).

[11] DIN EN ISO 15512:2019-09, Kunststoffe – Bestimmung des Wassergehaltes (ISO 15512:2003).

[12] Nelms, S. M. Inductively Coupled Plasma Mass Spectrometry Handbook. Blackwell Publishing Ltd.: Oxford, United Kingdom, 2005.

[13] Hill, S. J. Inductively coupled plasma spectrometry and its applications. In *Analytical chemistry*, 2nd ed.; Handley, A. J., Chalmers, J. M., Eds.; Blackwell Publishing Ltd.: Oxford, United Kingdom, 2006.

Die approbierte gedruckte Originalversion dieser Diplomarbeit ist an der TU Wien Bibliothek verfügbar
The approved original version of this thesis is available in print at TU Wien Bibliothek.

[14] Hagemann, R.; Nief, G.; Roth, E. Absolute isotopic scale for deuterium analysis of natural waters. Absolute D/H ratio for SMOW. *Tellus* **1970**, *22* (6), 712-715. DOI: 10.3402/tellusa.v22i6.10278 (acccessed 27.11.2022).

[15] Galbács, G.; Kéri, A.; Kálomista, I.; et al. Deuterium analysis by inductively coupled plasma mass spectrometry using polyatomic species: An experimental study supported by plasma chemistry modeling. *Anal Chim Acta* **2020**, *1104*, 28-37. DOI: 10.1016/j.aca.2020.01.011 (acccessed 13.10.2022).

[16] Russo, R. E.; Mao, X.; Gonzalez, J. J.; et al. Laser Ablation in Analytical Chemistry. *Analytical Chemistry* **2013**, *85* (13), 6162-6177. DOI: 10.1021/ac4005327 (acccessed 31.08.2022).

[17] Russo, R. E.; Mao, X. L.; Yoo, J.; et al. Chapter 3 - Laser ablation. In *Laser-Induced Breakdown Spectroscopy (Second Edition)*, Singh, J. P., Thakur, S. N. Eds.; Elsevier, 2007; pp 41-70.

[18] Miller, J. C.; Haglund, R. F. Laser ablation and desorption. In *Experimental Methods in the Physical Sciences*, Celotta, R., Lucatorto, T., Eds.; Academic Press: San Diego, 1997; Vol. 30.

[19] Koch, J.; Günther, D. Laser Ablation Inductively Coupled Plasma Mass Spectrometry. In *Encyclopedia of Spectroscopy and Spectrometry*, 2017; pp 526-532.

[20] Russo, R. E.; Mao, X.; Liu, H.; et al. Laser ablation in analytical chemistry—a review. *Talanta* **2002**, *57* (3), 425-451. DOI: 10.1016/S0039-9140(02)00053-X (acccessed 31.08.2022).

[21] Orellana, F. A.; Gálvez, C. G.; Orellana, F. A.; et al. Applications of laser-ablation-inductively-coupled plasma-mass spectrometry in chemical analysis of forensic evidence. *TrAC Trends in Analytical Chemistry* **2013**, *42*, 1-34. DOI: 10.1016/j.trac.2012.09.015 (acccessed 03.11.2022).

[22] Svelto, O. *Principles of Lasers*; Springer: New York, USA, 2010. DOI: 10.1007/978-1-4419-1302-9.

[23] Limbeck, A.; Bonta, M.; Nischkauer, W. Improvements in the direct analysis of advanced materials using ICP-based measurement techniques. *Journal of Analytical Atomic Spectrometry* **2017**, *32* (2), 212-232. DOI: 10.1039/c6ja00335d (acccessed 27.11.2022).

[24] Limbeck, A.; Galler, P.; Bonta, M.; et al. Recent advances in quantitative LA-ICP-MS analysis: challenges and solutions in the life sciences and environmental chemistry. *Anal Bioanal Chem* **2015**, *407* (22), 6593-6617. DOI: 10.1007/s00216-015-8858-0 (acccessed 27.11.2022).

[25] Wilschefski, S.; Baxter, M. Inductively Coupled Plasma Mass Spectrometry: Introduction to Analytical Aspects. *Clinical Biochemist Reviews* **2019**, *40* (3), 115-133. DOI: 10.33176/aacb-19-00024 (acccessed 21.10.2022).

Die approbierte gedruckte Originalversion dieser Diplomarbeit ist an der TU Wien Bibliothek verfügbar
The approved original version of this thesis is available in print at TU Wien Bibliothek.

[26] Yamada, N. Kinetic energy discrimination in collision/reaction cell ICP-MS: Theoretical review of principles and limitations. *Spectrochimica Acta Part B: Atomic Spectroscopy* **2015**, *110*, 31-44. DOI: 10.1016/j.sab.2015.05.008 (acccessed 03.11.2022).

[27] Tanner, S. D.; Baranov, V. I.; Bandura, D. R. Reaction cells and collision cells for ICP-MS: a tutorial review. *Spectrochimica Acta Part B: Atomic Spectroscopy* **2002**, *57* (9), 1361-1452. DOI: 10.1016/S0584-8547(02)00069-1 (acccessed 03.11.2022).

[28] Jamari, N. L. A.; Dohmann, J. F.; Raab, A.; et al. Novel non-target analysis of fluorine compounds using ICPMS/MS and HPLC-ICPMS/MS. *Journal of Analytical Atomic Spectrometry* **2017**, *32* (5), 942-950. DOI: 10.1039/c7ja00051k (acccessed 13.10.2022).

[29] Jamari, N. L. A.; Behrens, A.; Raab, A.; et al. Plasma processes to detect fluorine with ICPMS/MS as [M–F]+: an argument for building a negative mode ICPMS/MS. *Journal of Analytical Atomic Spectrometry* **2018**, *33* (8), 1304-1309. DOI: 10.1039/c8ja00050f (acccessed 13.10.2022).

[30] Jamari, N. L. A.; Dohmann, J. F.; Raab, A.; et al. Novel non-targeted analysis of perfluorinated compounds using fluorine-specific detection regardless of their ionisability (HPLC-ICPMS/MS-ESI-MS). *Anal Chim Acta* **2019**, *1053*, 22-31. DOI: 10.1016/j.aca.2018.11.037 (acccessed 14.10.2022).

[31] Elemental Scientific Lasers. *ESL213 Laser Ablation System | Micro*. 2022. Available at: https://www.icpmslasers.com/laserablation/nwr213/ (accessed 30.11.2022).

[32] Applied Spectra. *J200 Tandem LA-LIBS Instrument*. 2022. Available at: https://appliedspectra.com/products/j200-tandem-libs-la.html (accessed 30.11.2022).

[33] Rutgers (The State University of New Jersey). *Thermo ICAP-Q*. 2016? Available at: https://rial.marine.rutgers.edu/instruments/thermo-icap-q/ (accessed 30.11.2022).

[34] Gurevich, E. L.; Hergenröder, R. A simple laser ICP-MS ablation cell with wash-out time less than 100 ms. *Journal of Analytical Atomic Spectrometry* **2007**, *22* (9), 1043-1050, 10.1039/B704700B. DOI: 10.1039/B704700B (acccessed 27.11.2022).

[35] Boulyga, S. F. Calcium isotope analysis by mass spectrometry. *Mass Spectrometry Reviews* **2010**, *29* (5), 685-716. DOI: 10.1002/mas.20244 (acccessed 21.11.2022).

[36] Farkaš, J. Calcium Isotopes. In *Encyclopedia of Geochemistry: A Comprehensive Reference Source on the Chemistry of the Earth*, White, W. M. Ed.; Springer International Publishing, 2018; pp 181-186.

[37] Frick, D. A.; Günther, D. Fundamental studies on the ablation behaviour of carbon in LA-ICP-MS with respect to the suitability as internal standard. *Journal of Analytical Atomic Spectrometry* **2012**, *27* (8), 1294. DOI: 10.1039/c2ja30072a (acccessed 23.11.2022).

Die approbierte gedruckte Originalversion dieser Diplomarbeit ist an der TU Wien Bibliothek verfügbar
The approved original version of this thesis is available in print at TU Wien Bibliothek.

[38] Deiting, D.; Börno, F.; Hanning, S.; et al. Investigation on the suitability of ablated carbon as an internal standard in laser ablation ICP-MS of polymers. *Journal of Analytical Atomic Spectrometry* **2016**, *31* (8), 1605-1611. DOI: 10.1039/c6ja00020g (acccessed 23.11.2022).

[39] Makino, Y.; Nakazato, T. Determination of trace elements in polymers using fsLA-ICP-MS with internal standardization by carbon. *Journal of Analytical Atomic Spectrometry* **2021**, *36* (9), 1895-1899. DOI: 10.1039/d1ja00198a (acccessed 23.11.2022).

[40] Osswald, T. A.; Baur, E.; Brinkmann, S.; et al. Material Property Tables. *International Plastics Handbook* **2006**, 717-902. DOI: 10.3139/9783446407923.bm (acccessed 25.11.2022).

[41] Mao, X. L.; Borisov, O. V.; Russo, R. E. Enhancements in laser ablation inductively coupled plasma-atomic emission spectrometry based on laser properties and ambient environment. *Spectrochimica Acta Part B: Atomic Spectroscopy* **1998**, *53* (5), 731-739. DOI: 10.1016/S0584-8547(98)00106-2 (acccessed 27.11.2022).

[42] Bogaerts, A.; Chen, Z.; Bleiner, D. Laser ablation of copper in different background gases: comparative study by numerical modeling and experiments. *Journal of Analytical Atomic Spectrometry* **2006**, *21* (4). DOI: 10.1039/b514313f (acccessed 27.11.2022).

[43] Jacob, J.; Shanmugavelu, P.; Balasubramaniam, R.; et al. Study and Analysis of the Thermal Effects during the Excimer Laser Ablation of Polymers with Different Gaseous Environment. In *5th International and 26th All India Manufacturing Technology, Design and Research Conference (AIMTDR 2014)*, Guwahati, India, 12.-14.12.2014. Available at: https://www.iitg.ac.in/aimtdr2014/PROCEEDINGS/papers/331.pdf (accessed 26.11.2022).

[44] Urech, L.; Lippert, T. Designed Polymers for Ablation. In *Laser Ablation and its Applications*, Phipps, C. Ed.; Optical Sciences, Springer, 2007.

[45] Lin, J.; Liu, Y.; Yang, Y.; et al. Calibration and correction of LA-ICP-MS and LA-MC-ICP-MS analyses for element contents and isotopic ratios. *Solid Earth Sciences* **2016**, *1* (1), 5-27. DOI: 10.1016/j.sesci.2016.04.002 (acccessed 27.11.2022).

[46] Vanhaecke, F.; Vanhoe, H.; Dams, R.; et al. The use of internal standards in ICP-MS. *Talanta* **1992**, *39* (7), 737-742. DOI: 10.1016/0039-9140(92)80088-U (acccessed 27.11.2022).

[47] Mcmillen, D. F.; Golden, D. M. Hydrocarbon Bond Dissociation Energies. *Annual Review of Physical Chemistry* **1982**, *33* (1), 493-532. DOI: 10.1146/annurev.pc.33.100182.002425 (acccessed 16.11.2022).

[48] Davico, G. E.; Bierbaum, V. M.; Depuy, C. H.; et al. The C-H Bond Energy of Benzene. *Journal of the American Chemical Society* **1995**, *117* (9), 2590-2599. DOI: 10.1021/ja00114a023 (acccessed 16.11.2022).

Die approbierte gedruckte Originalversion dieser Diplomarbeit ist an der TU Wien Bibliothek verfügbar
The approved original version of this thesis is available in print at TU Wien Bibliothek.

[49] Gilormini, P.; Verdu, J. On the role of hydrogen bonding on water absorption in polymers. *Polymer* **2018**, *142*, 164-169. DOI: 10.1016/j.polymer.2018.03.033 (acccessed 27.11.2022).

[50] Grabowski, S. J. Hydrogen bonding strength—measures based on geometric and topological parameters. *Journal of Physical Organic Chemistry* **2004**, *17* (1), 18-31. DOI: 10.1002/poc.685 (acccessed 17.11.2022).

[51] Schroeder, L. R.; Cooper, S. L. Hydrogen bonding in polyamides. *Journal of Applied Physics* **1976**, *47* (10), 4310-4317. DOI: 10.1063/1.322432 (acccessed 19.11.2022).

[52] David, V.; Grinberg, N.; Moldoveanu, S. C. Long-Range Molecular Interactions Involved in the Retention Mechanisms of Liquid Chromaography. In *Advances in Chromatography: Volume 54*, 1st ed.; CRC Press, 2017.

[53] Lee, W.-J.; Chang, J.-G.; Ju, S.-P. Hydrogen-Bond Structure at the Interfaces between Water/Poly(methyl methacrylate), Water/Poly(methacrylic acid), and Water/Poly(2-aminoethylmethacrylamide). *Langmuir* **2010**, *26* (15), 12640-12647. DOI: 10.1021/la904898v (acccessed 19.11.2022).

[54] Serbezeanu, D.; Homocianu, M.; Macsim, A. M.; et al. Flexible thin films based on poly(ester imide) materials for optoelectronic applications. *Polymer International* **2022**, *71* (1), 98-106. DOI: 10.1002/pi.6288 (acccessed 2022-11-30T17:18:26).

[55] Majumder, M.; Rendall, C. S.; Eukel, J. A.; et al. Overcoming the "Coffee-Stain" Effect by Compositional Marangoni-Flow-Assisted Drop-Drying. *The Journal of Physical Chemistry B* **2012**, *116* (22), 6536-6542. DOI: 10.1021/jp3009628 (acccessed 28.11.2022).

[56] Li, Y.; Diddens, C.; Segers, T.; et al. Evaporating droplets on oil-wetted surfaces: Suppression of the coffee-stain effect. *Proceedings of the National Academy of Sciences* **2020**, *117* (29), 16756-16763. DOI: 10.1073/pnas.2006153117 (acccessed 28.11.2022).

[57] Li, H.; Buesen, D.; Williams, R.; et al. Preventing the coffee-ring effect and aggregate sedimentation by in situ gelation of monodisperse materials. *Chemical Science* **2018**, *9* (39), 7596-7605. DOI: 10.1039/c8sc03302a (acccessed 28.11.2022).

[58] Petrelli, M.; Laeger, K.; Perugini, D. High spatial resolution trace element determination of geological samples by laser ablation quadrupole plasma mass spectrometry: implications for glass analysis in volcanic products. *Geosciences Journal* **2016**, *20* (6), 851-863. DOI: 10.1007/s12303-016-0007-z (acccessed 28.11.2022).

[59] Gardner, R. J.; Martin, J. R. Humid aging of plastics: Effect of molecular weight on mechanical properties and fracture morphology of polycarbonate. *Journal of Applied Polymer Science* **1979**, *24* (5), 1269-1280. DOI: 10.1002/app.1979.070240512 (acccessed 29.11.2022).

Die approbierte gedruckte Originalversion dieser Diplomarbeit ist an der TU Wien Bibliothek verfügbar
The approved original version of this thesis is available in print at TU Wien Bibliothek.

[60] Sihvo, V.; Pyrhonen, J. Steam-Resistivity of Wire Insulating Materials. In *2007 IEEE Lausanne Power Tech*, 2007. DOI: 10.1109/pct.2007.4538288. Available at: https://ieeexplore.ieee.org/document/4538288 (accessed 29.11.2022).

[61] Jacques, B.; Werth, M.; Merdas, I.; et al. Hydrolytic ageing of polyamide 11. 1. Hydrolysis kinetics in water. *Polymer* **2002**, *43* (24), 6439-6447. DOI: 10.1016/S0032-3861(02)00583-9 (acccessed 29.11.2022).

[62] Touris, A.; Turcios, A.; Mintz, E.; et al. Effect of molecular weight and hydration on the tensile properties of polyamide 12. *Results in Materials* **2020**, *8*, 100149. DOI: 10.1016/j.rinma.2020.100149 (acccessed 29.11.2022).

Die approbierte gedruckte Originalversion dieser Diplomarbeit ist an der TU Wien Bibliothek verfügbar
The approved original version of this thesis is available in print at TU Wien Bibliothek.